JAMES | Journal of Advances in Modeling Earth Systems

RESEARCH ARTICLE
10.1029/2019MS001925

Special Section:
Community Earth System Model version 2 (CESM2) Special Collection

Land Use and Land Cover Change Strongly Modulates Land-Atmosphere Coupling and Warm-Season Precipitation Over the Central United States in CESM2-VR

Anjana Devanand[1,2,3], Maoyi Huang[1,4], David M. Lawrence[5], Colin M. Zarzycki[5,6], Zhe Feng[1], Peter J. Lawrence[2], Yun Qian[1], and Zhao Yang[1]

[1]Atmospheric Sciences and Global Change Division, Pacific Northwest National Laboratory, Richland, WA, USA, [2]Interdisciplinary Programme in Climate Studies, Indian Institute of Technology, Bombay, India, [3]Now at School of Civil, Environmental and Mining Engineering, University of Adelaide, [4]Now at Office of Science and Technology Integration, National Weather Service, National Oceanic and Atmospheric Administration, [5]National Center for Atmospheric Research, Boulder, CO, USA, [6]Department of Meteorology and Atmospheric Science, Penn State University, State College, PA, USA

Abstract Prior research indicates that land use and land cover change (LULCC) in the central United States has led to significant changes in surface climate. The spatial resolution of simulations is particularly relevant in this region due to its influence on model skill in capturing mesoscale convective systems (MCSs) and on representing the spatial heterogeneity. Recent advances in Earth system models (ESMs) make it feasible to use variable resolution (VR) meshes to study regional impacts of LULCC while avoiding inconsistencies introduced by lateral boundary conditions typically seen in limited area models. Here, we present numerical experiments using the Community Earth System Model version 2–VR to evaluate (1) the influence of resolution and land use on model skill and (2) impacts of LULCC over the central United States at different resolutions. These simulations are configured either on the 1° grid or a VR grid with grid refinement to 1/8° over the contiguous United States for the period of 1984–2010 with two alternative land use data sets corresponding to the preindustrial and present day states. Our results show that skill in simulating precipitation over the central United States is primarily dependent on resolution, whereas skill in simulating 2-m temperature is more dependent on accurate land use. The VR experiments show stronger LULCC-induced precipitation increases over the Midwest in May and June, corresponding to an increase in the number of MCS-like features and a more conductive thermodynamic environment for convection. Our study demonstrates the potential of using VR ESMs for hydroclimatic simulations in regions with significant LULCC.

Plain Language Summary Land use and land cover change (LULCC) in the central United States has likely affected the historical climate of this region, along with other global and regional factors. Experiments using Earth system models can be used to understand how LULCC has affected the regional climate. But such studies are limited by model resolution used for the experiments. Recent developments in Earth system modeling allow for higher regional resolution simulations over areas of focused interest in global simulations. In this study, we perform model experiments using the Community Earth System Model at a high resolution over the central United States to understand how resolution affects the model skill and the simulated LULCC impacts. The warm-season precipitation over the central United States shows lower biases in the high-resolution simulations. We also find stronger precipitation increases over the Midwest during May and June due to LULCC in experiments at high resolution. This is because the environmental conditions over the Midwest become more favorable for convective activities as a result of LULCC in the high-resolution experiments.

Key Points:
- Precipitation and temperature biases over the central United States are reduced with more accurate land use and higher resolution in VR-CESM
- The high-resolution model shows stronger LULCC-induced precipitation increases over the Midwest in May and June
- Variable resolution model demonstrates great potential to be used for regional hydroclimatic applications in areas of major LULCC

Supporting Information:
- Supporting Information S1

Correspondence to:
M. Huang,
maoyi.huang@pnnl.gov

Citation:
Devanand, A., Huang, M., Lawrence, D. M., Zarzycki, C. M., Feng, Z., Lawrence, P. J., et al. (2020). Land use and land cover change strongly modulates land-atmosphere coupling and warm-season precipitation over the central United States in CESM2-VR. *Journal of Advances in Modeling Earth Systems*, *12*, e2019MS001925. https://doi.org/10.1029/2019MS001925

Received 17 OCT 2019
Accepted 8 JUN 2020
Accepted article online 11 JUN 2020

1. Introduction

Land use and land cover change (LULCC) influences the Earth system through biogeophysical (Mahmood et al., 2014; Pielke et al., 2011; Pitman et al., 2009) and biogeochemical (Lawrence et al., 2012; Unger, 2014) feedbacks. The primary biogeophysical feedback is a global net increase in surface albedo and changes in

surface energy partitioning due to deforestation (Davin & de Noblet-Ducoudré, 2010; Lawrence & Chase, 2010; Lee et al., 2011) with respect to the historical period. Biogeochemical feedbacks stem from changes in terrestrial carbon pools resulting in changes in emissions from the land surface (Lawrence et al., 2012, 2018; Shevliakova et al., 2009; Unger, 2014). LULCC has been recognized as an important anthropogenic forcing on the Earth system (Feddema et al., 2005; Hibbard et al., 2017), and several model intercomparison projects have been conducted or are underway aiming at understanding LULCC impacts (e.g., "Land-Use and Climate, IDentification of robust impacts" [LUCID], Pitman et al., 2009; and "Land Use Model Intercomparison Project" [LUMIP], Lawrence et al., 2016). The present consensus indicates that the global mean signal of LULCC-induced effects balance each other, resulting in insignificant global mean changes, partly because the surface warming induced by the biogeochemical feedbacks are offset by the cooling induced by biogeophysical feedbacks (Brovkin et al., 2013; Myhre et al., 2013). However, LULCC is a dominant forcing in areas of major land use transitions, potentially resulting in stronger local to regional feedbacks than that caused by the global warming signal in these regions and affecting both mean and extremes of regional hydroclimate (Findell et al., 2017; Y. Li et al., 2015; Seneviratne et al., 2018). These regional LULCC signals are as yet poorly understood and often lack model consensus in terms of the sign of changes in latent heat flux and Bowen ratio (Lejeune et al., 2017; Li et al., 2018; Pitman et al., 2009; Yang et al., 2016) and the mechanisms behind these changes, necessitating more thorough analysis of land parameterizations in coupled Earth system simulations of individual models and their responses to LULCC perturbations (de Noblet-Ducoudré et al., 2012).

The central United States is a region that has experienced significant LULCC since the preindustrial period. The primary changes over this region are the expansion and intensification of rainfed and irrigated crop lands for agriculture. The area witnessed a rapid expansion of farmlands from 1900 to the 1950s (Parton et al., 2007), with technological advances and favorable changes in extreme temperature and length of the growing season (Butler et al., 2018; Kucharik et al., 2010) enhancing the crop productivity and yield from these agricultural lands post 1950s (Andresen et al., 2012; Parton et al., 2007). The central United States is also a "hotspot" of land-atmosphere coupling during the warm season (Koster et al., 2004; Mei et al., 2012) with land surface processes exerting a relatively strong influence on regional hydroclimate. Consequently, LULCC has likely influenced the historical changes in mean and extremes of temperature and precipitation over this region (Alter et al., 2018; Chen et al., 2017; Mueller et al., 2016). In addition, global warming signals are also perceived to have effects on some aspects of warm-season climate of this region (Diffenbaugh et al., 2011; Prein et al., 2017). The complex interplay of global signals with the regional forcing of LULCC thus necessitates the use of model simulations to understand the separate influences of these forcings and the mechanisms behind them.

The spatial resolution of Earth system model (ESM) simulations over the central United States may affect the simulated LULCC impacts and model skill in simulating warm season climate. Changes in land surface, such as establishment of new cropping systems and irrigation, typically occur on small spatial scales that may require modeling at finer resolutions to fully capture their spatial variability. In addition, persistent warm temperature and dry precipitation biases over this region exist in both weather and climate scale simulations at different resolutions (Klein et al., 2006; Van Weverberg et al., 2018). The biases are reported to be linked to underrepresentation of mesoscale convective systems (MCSs), deficiencies in representing shallow convection, and biases in land processes (Cheinet et al., 2005; Cheruy et al., 2014; Klein et al., 2006; Lin et al., 2017; Morcrette et al., 2018; Qian et al., 2013; Van Weverberg et al., 2018; Yang et al., 2019). These pathways are coupled and act simultaneously.

Parallelly, modeling studies at convection permitting resolutions provide more insights into the biases associated with the simulation of convective systems (Prein et al., 2015). The representation of cloud microphysical processes influences the vertical velocity of updrafts and the precipitation rates by affecting the cloud ice content in the atmosphere (Fan et al., 2017; Varble et al., 2014). Further, feedback from convective systems affects both convective-scale dynamics and microphysical properties such as rainfall amount (Feng et al., 2018; Yang et al., 2017). Representations of these processes are sensitive to model horizontal resolution. Model experiments at a finer resolution partly alleviate these biases, which is attributed to their ability to better capture MCSs over the central United States (Feng et al., 2018; Prein et al., 2017; Yang et al., 2017). The warm season precipitation over the central United States is dominated by contributions from MCSs that account for 40–60% of the total April to September rainfall in observations (Feng et al., 2016; Jiang

et al., 2006). MCS frequency and intensity in the past 35 years in observations (Feng et al., 2016) are expected to intensify further in a warming climate, resulting in an increase in flood risk (Prein, Liu, Ikeda, Bullock, et al., 2017). Modeling MCS activities and understanding the LULCC-induced changes in these systems is thus of relevance both for advancing model skill and for characterizing the impacts of changes in these systems.

Traditionally, regional models that offer the capability to perform experiments at requisite fine resolutions have been used to study the impact of LULCC on regional climate over the contiguous United States (hereafter CONUS) (Alter et al., 2018; Diffenbaugh, 2009). The development of variable resolution (VR) meshes in global ESMs offers a new alternative that can be used to perform consistent high-resolution regional simulations for such studies. VR meshes eliminate inconsistencies introduced by the use of lateral boundary conditions and differences in physics parameterizations between the parent and regional models. They offer a new tool for regional analyses using simulations that allow for two-way upscale flow interactions and global conservation of quantities in climate simulations. The VR mesh over CONUS in the Community Earth System Model (CESM) is a part of the available model configuration suite, and this development allows us to use CESM for regional experiments. In this study, we aim to demonstrate the effectiveness of this tool for studying biogeophysical feedbacks between LULCC and regional climate with forcings (e.g., emission and land use) that are consistent with other regions globally.

Specifically, we use the VR configuration of CESM to perform experiments to understand the impact of LULCC over the central United States and the resolution dependence of simulated impacts. VR meshes in CESM have previously been employed to study regional climate features over the western United States and tropical cyclones in the Atlantic (Rhoades et al., 2018; Wu et al., 2017; Zarzycki & Jablonowski, 2014). It has been demonstrated that CESM2-VR is capable of capturing the global climatology of the uniform coarse-resolution simulations while reproducing observed extreme climate statistics over the region of grid refinement, for example, the CONUS (Gettelman et al., 2018; Zarzycki et al., 2014). We use a suite of CESM2 experiments with and without grid refinement to understand (1) how the persistent warm-dry biases over the central United States are influenced by land use representation compared to by model resolution, (2) the impacts of LULCC on warm-season climate, and (3) the resolution dependence of these simulated impacts.

2. Experiment Design

2.1. CESM Configurations

We perform experiments using the CESM version 2 (CESM2) to understand impacts of LULCC on regional climate over the central United States and the dependence of the simulated impacts on the model resolution. The CESM configuration used in this study consists of the Community Atmospheric Model version 6 (CAM6) Spectral element (SE) as the atmospheric component and the Community Land Model version 5 (CLM5, Lawrence et al., 2019) as the land component. Descriptions of the SE dynamical core in CAM6 and the associated physics suite in CESM2 are documented in Lauritzen et al. (2018) and Gettelman et al. (2018). In CAM6, deep convection is represented using the Zhang McFarlene convective scheme, which uses a plume ensemble approach to parameterize subgrid scale convection (Zhang & McFarlane, 1995). The "Cloud Layers Unified by Binormals" (CLUBB) model is used to represent boundary layer turbulence, shallow convection, and cloud macrophysics (Bogenschutz et al., 2013; Golaz et al., 2002). A two-moment cloud microphysics scheme, MG2 (Gettelman & Morrison, 2015), is used to calculate the mass and number concentrations of condensed species, rain, and snow. The development of physics suite in CESM2 has focused on the development of "scale-insensitive" physical parameterizations (Gettelman et al., 2018). The physical parameterization suite in CAM5 and CAM6 are found to be relatively insensitive to changes in horizontal resolution with respect to cloud cover and radiation feedback in aqua planet simulations (Gettelman et al., 2018). In addition, full physics simulations using the VR model reveal that the model is capable of capturing high-frequency, high-resolution statistics in the area of grid refinement. Thus, CESM-VR is a viable alternative to traditional nesting for regional studies.

The experiments performed in this study follow the Atmospheric Model Intercomparison Project (AMIP) protocol for the historical period and use prescribed sea surface temperatures (SSTs), solar variations, and aerosol chemistry during the years 1979 to 2010 (Gates et al., 1999). That is, the two experiments are

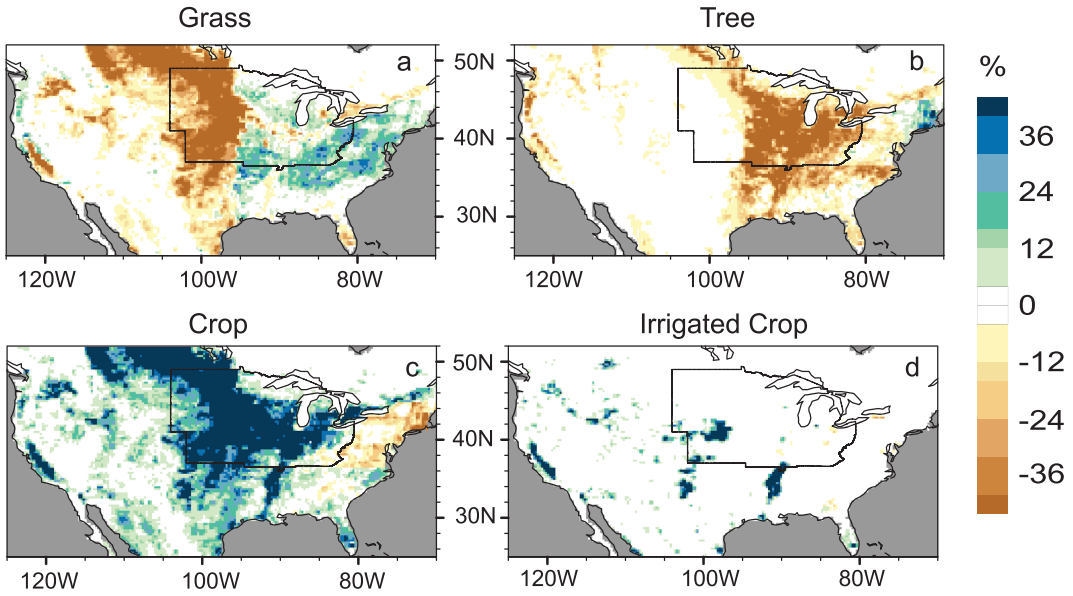

Figure 1. Land use land cover change (LU2000 minus LU1850 in %) (a) grass, (b) tree, (c) crop, and (d) irrigated crop.

identical in all other aspects and only differ in the prescribed LULC to study the impact of LULCC on regional climate. We use two alternate LULC gridded data layers corresponding to different time periods (see details below). The SST and land use data sets used in these experiments are the default historical data sets used for CESM2 simulations. The land use data sets are derived from the Land Use Harmonization 2 (LUHv2) data set (Hurtt et al., 2018), which has a spatial resolution of 0.25°. The terrestrial biogeochemical cycle (BGC) and crop modules within CLM5 are turned on to prognostically simulate vegetation characteristics and terrestrial carbon and nitrogen cycles. The model simulations are initialized in year 1979 using spun-up equilibrated land initial conditions from CESM2 control simulations. We discard the first 5 years as the spin-up period to allow the vegetation state to come to quasi-equilibrium with the prescribed fixed LULC data. Both sets of simulations are initialized from the same spun-up land states from the end of a CLM5 historical simulation for the years 1850 to 2015 with LULCC transitions at a resolution of 1°. The initial conditions are interpolated to the SE grids by the land model for the land-atmosphere simulations presented here. We present the warm-season leaf area index (LAI) in CONUS from the full 32 years (5 years spin-up + 27 years) of simulations in Figure S1 in the supporting information. Simulated LAIs do not show significant trends except that a weak negative trend is found in one simulation. We expect that a small drift is likely to remain due to the short spin-up period used for these simulations, but the high computational costs of the VR simulations prohibit us from a longer spin-up. Additionally, in separate land-only tests, we found that when initializing the model from a previously spun-up state, the LAI state came into quasi-equilibrium within about 5–15 years. For our analysis here, we erred on the lower end of the spin-up time in order to maintain sufficient years for a climatological analysis. The analyses presented in this study therefore uses model output corresponding to 27 years from 1984 to 2010.

To study the regional impacts of LULCC, we perform model experiments using two alternate LULC data sets corresponding to the preindustrial (year 1850) and present day (year 2000) time periods. The experiments use fixed land use maps corresponding to these two years without land use transitions. The preindustrial land use corresponding to year 1850 (hereafter LU1850) depicts the historical natural vegetation over the CONUS, wherein the eastern half of the country is dominated by trees and the western half by grasses. The present-day land use corresponding to the year 2000 (hereafter LU2000) has an expansion of cropland over the central United States (Figure S2). The irrigated cropland over the central United States contributes to a small proportion of the total cropland expansion (Figure S2). Figures 1a–1d show the differences in land use as percentages of the total grid cell area between the preindustrial and present-day conditions (i.e., LU2000 minus LU1850). The CESM experiments that differ only in the prescribed land use (LU1850 vs.

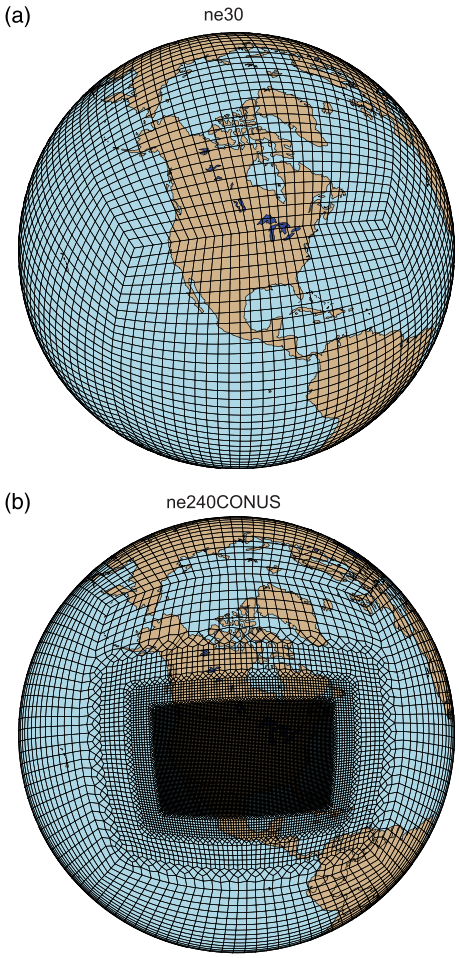

Figure 2. The CESM2 SE grids at resolutions of (a) ne30 (1°, ~111 km) and (b) ne240CONUS (1/8°/~14 km over the CONUS and 1°/~111 km otherwise). The figure shows the CAM-SE dynamics grids and the resolution of CLM, and the CAM physics is a 3 × 3 collocation grid within each cell.

LU2000) are used to understand the impact of LULCC on regional climate. Since the experiments correspond to the historical period (1984–2010), LU2000 is a more accurate representation of the land conditions during this period. The comparison of LU2000 and LU1850 simulations with observations thus also enables us to quantify the influence of land use representation on the model skill.

In order to address the variation in model skill with resolution and to understand the resolution dependence of the simulated LULCC impacts, the experiment suite is designed to use model grids at two different spatial resolutions, ne30 and ne240CONUS (Figures 2a and 2b). The ne30 grid is a uniform SE global grid with an equivalent resolution of ~1°. The ne240CONUS is a VR SE grid with regional refinement to 1/8° (~14 km) over the CONUS. The experiments include three sets of LULCC experiments (i.e., LU1850 versus LU2000 simulations) using different combinations of the ne30 and ne240CONUS land and atmosphere grids, listed in Table 1. The first experiment set (Table 1, Sl. No. 1 and 2) uses uniform coarse-resolution (~1°) land and atmosphere grids, hereafter LLAL (low-resolution land–low-resolution atmosphere). In the second set of experiments (Table 1, Sl. No. 3 and 4), the land component uses the ne240CONUS VR grid while the atmospheric component uses the ne30 grid, which represent a coarse-resolution atmosphere coupled to a fine-resolution land grid, hereafter LHAL (high-resolution land–low-resolution atmosphere). The third set of experiments (Table 1, Sl. No. 5 and 6) uses the ne240CONUS VR grid for both the atmosphere and land components, hereafter LHAH (high-resolution land–high-resolution atmosphere). The experiment suite therefore includes a total of six simulations, using the three grid combinations with prescribed LULC data for the two different time periods, LU1850 and LU2000. Overall, the experiment suite is designed to understand the relative importance of land and atmospheric resolutions in (1) model skill in capturing the characteristics of regional climate and (2) simulating the climate effects of LULCC over the central United States.

The model outputs generated by the fine-resolution experiments (LHAH) pose a challenge in terms of data storage of fine temporal resolution outputs from the full set of simulated variables. This requires careful consideration and optimization of the temporal output frequency of the output variables given computational and data storage constraints. The simulations were configured to save outputs of relevant land and

Table 1
LULCC Experiments Using CESM2

Sl. No.	Experiment name	Atmosphere resolution (CONUS)	Land resolution (CONUS)	Land use
1	LLAL_LU2000 (low-resolution land coupled to low-resolution atmosphere)	1° (~111 km)	1° (~111 km)	LU2000
2	LLAL_LU1850 (low-resolution land coupled to low-resolution atmosphere)	1° (~111 km)	1° (~111 km)	LU1850
3	LHAL_LU2000 (high-resolution land coupled to low-resolution atmosphere)	1° (~111 km)	1/8° (~14 km)	LU2000
4	LHAL_LU1850 (high-resolution land coupled to low-resolution atmosphere)	1° (~111 km)	1/8° (~14 km)	LU1850
5	LHAH_LU2000 (high-resolution land coupled to high-resolution atmosphere)	1/8° (~14 km)	1/8° (~14 km)	LU2000
6	LHAH_LU1850 (high-resolution land coupled to high-resolution atmosphere)	1/8° (~14 km)	1/8° (~14 km)	LU1850

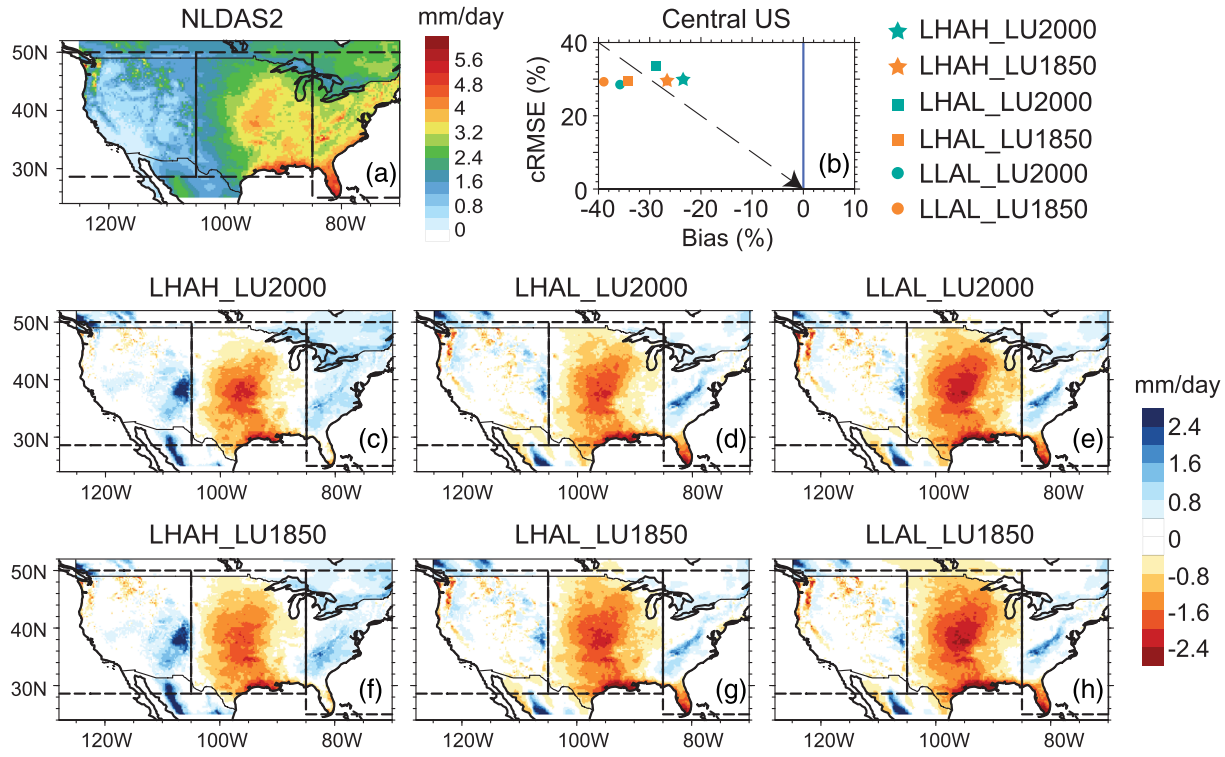

Figure 3. (a) Warm-season (AMJJA) precipitation climatology (in mm/day) during 1984 to 2010 based on NLDAS; (b) regional precipitation biases and cRMSE over the central United States (in %). The arrow points toward increasing skill. (c–e) Precipitation biases in experiments using LU2000 at resolutions LHAH, LHAL, and LLAL, respectively (in mm/day). (f–h) Precipitation biases in experiments using LU1850 at resolutions LHAH, LHAL, and LLAL respectively (in mm/day). The dashed lines show regions eastern, central, and western United States over which the regional errors statistics are calculated.

atmosphere variables at daily temporal resolution. Further, we saved subdaily outputs from these experiments for a subset of the total simulation period. The LHAH experiments were configured to output hourly precipitation in addition to the original output variable list from 1 January 1999 to 31 December 2010. This enables us to track and analyze MCS-like precipitation features in these experiments. All experiments were configured to output instantaneous 6-hourly 3-D atmospheric variables from 1 January 2007 to 31 December 2010. These additional outputs enable us to analyze changes in thermodynamic environment that lead to the LULCC-induced land-atmosphere coupling strength and precipitation changes.

2.2. Methods Used for Model Evaluation and Analysis

We evaluate the model skill in capturing precipitation and 2-m air temperature (T-2 m) over CONUS during the warm season (April to August). The National Land Data Assimilation System version 2 (NLDAS2) data for the 27-year period corresponding to the experiments (1984 to 2010) is used as the reference data set for benchmarking precipitation from the model experiments. We benchmarked the 2-m air temperature (T-2 m) by comparing the simulations with the Parameter-elevation Regressions on Independent Slopes Model (PRISM) data set. We use area-weighted mean monthly regional bias and centered root mean square error (cRMSE) of 27 years (1984 to 2010) to quantify errors in the model experiments over different regions, that is, the eastern, central and western United States marked using dashed lines in Figure 3. The area-weighted regional mean warm-season precipitation and T-2 m from the model experiments are compared with the area-weighted regional mean estimates from the observational data sets to calculate the regional mean bias. The cRMSE are calculated as the root mean square errors of the anomalies after removing the respective mean warm-season climatology from observations and simulations. The cRMSE provide an estimate of the model skill in simulating the seasonal cycle of precipitation and T-2 m.

All model outputs were interpolated to the 1/8° NLDAS grid using bilinear interpolation for evaluation and analysis. The SE grids used in our experiments are unstructured meshes that require the outputs to be

interpolated to regular grids for analysis. We interpolate all experiments (LLAL, LHAL, and LHAH) to the NLDAS grid in order to avoid differences in the analysis that would otherwise occur as a result of differences in the number of grid cells between them. The comparison of experiments at different resolutions presented here thus highlight the added value of Earth system modeling at high resolution versus interpolation of coarser resolution model outputs to a high-resolution grid. We use the two tailed *t* test to assess the significance of the LULCC-induced changes in daily fields for each month and report results at the 5% significance level unless otherwise specified.

2.2.1. PF Tracking Algorithm

We track MCS-like features in the LHAH experiments using the Precipitation Feature (PF) algorithm developed by Feng et al. (2016). The PF algorithm uses hourly precipitation from the experiments to track contiguous precipitation features in space and time to identify MCS-like features. The algorithm was developed based on historical MCSs identified from satellite brightness temperatures used in conjunction with NLDAS precipitation data for the same period (Feng et al., 2016). To develop the algorithm, Feng et al. (2016) identified MCSs from satellite data based on the size and lifetime of contiguous cold cloud shields. The corresponding precipitation characteristics of these MCSs were calculated from the NLDAS data and used to develop the PF tracking algorithm that characterizes and identifies MCSs based on precipitation data alone. The PF algorithm tracks PF features in space and time and identifies MCSs from PFs with major axis length exceeding 200 km that persists for at least 4 hr. In addition, the algorithm uses three additional MCS lifetime dependent precipitation characteristics to identify MCSs—the PF maximum area, maximum areal mean rain rate, and maximum skewness of pixel-level rain rates. Feng et al. (2016) identified the threshold values of these three characteristics for a PF to be classified as an MCS. We employ the same thresholds to identify MCS-like features in the LHAH experiments. Note that the PF threshold values used to define MCS-like features depend on resolution, as they are derived from 1/8° grid (~12 km) NLDAS data. Tracking of MCS-like features with coarser resolution data such as our 1° model outputs is currently not feasible.

2.2.2. Land-Atmosphere Coupling Indices

The coupling between these land and atmospheric variables are too complex to be characterized using simplistic linear relationships. However, statistical coupling indices have proved useful to quantify the strength of influence of causally related variables within the land-atmosphere system. While these indices do not rely on the physical formulations of processes, they quantify the "sensitivity" or "strength" of land-atmosphere coupling in model and observation-based data sets (Dirmeyer, 2011). Here we employ statistical indices of land-atmosphere coupling developed in literature to characterize the strength of coupling in our simulations and the changes in coupling strength due to LULCC. This analysis is undertaken to understand the differences in land-atmosphere coupling strength in simulations at different resolutions. We hypothesize that changes in coupling strength may influence atmospheric states and hence MCS activities in the simulations.

We quantify the strength of land-atmosphere coupling in the experiments using statistical two-legged coupling metrics applied in previous observational and model based analyses (Dirmeyer, 2011; Dirmeyer et al., 2018). Two-legged coupling metrics employ correlations between land surface states, surface fluxes, and atmospheric states to quantify the strength of the terrestrial and atmospheric legs of the land-atmosphere feedback. The terrestrial leg of this feedback uses the land surface state as the driving variable and the surface fluxes as the response variable, while the atmospheric leg uses surface fluxes as driving variable and atmospheric state as the response variable. The metrics also incorporate the variance in the driving variable to ensure that it has sufficient variability in time to result in a change in the response variable. The coupling index I between a driving variable a and response variable b, $I = \sigma(a)\frac{db}{da} = r(a, b)\sigma(b)$, where σ is the standard deviation of the variable in time, r is correlation in time, and $\frac{db}{da}$ is the slope of the least square linear regression fit line describing b dependent on a (Dirmeyer, 2011; Dirmeyer et al., 2018). We calculate these indices using daily data grouped by month. Indices are calculated only for grids that show significant correlations between the driving and response variables at 5% significance level. We analyze the differences in coupling strength of the terrestrial and atmospheric legs at different resolutions and the changes in coupling strength induced by LULCC using only grids that show significant coupling strength in both the LU2000 and LU1850 experiments.

We use two terrestrial coupling indices, which employ daily LAI and soil moisture in the top 10 cm of the soil (SW) as the driving variables and SH as the response variable. The strength of the terrestrial leg is quantified as the influence of daily land surface states (LAI and SW) on SH, defined as $\sigma(SH) \cdot r(LAI, SH)$ and $\sigma(SH) \cdot r(SW, SH)$. In grids covered with vegetation, LAI would have a strong influence on the surface fluxes. The correlations of LAI and SH ($r(LAI, LH)$) are expected to be negative since an increase in LAI would have a negative effect on SH through increasing evapotranspiration. We find stronger correlations between LAI and surface fluxes compared to the correlations between SW and surface fluxes over the Midwest during May and June, as a result of dense preindustrial vegetation coverage and present-day agricultural intensification. This is consistent with previous observational and model-based studies (Williams et al., 2016; Williams & Torn, 2015). In the grid cells containing larger proportions of bare land, SW would have a stronger influence on the surface fluxes. The correlations of SW and SH are expected to be negative because a higher soil moisture would result in more evaporation reducing SH.

We use SH as the forcing variable and LCL as the response variable to calculate the strength of the atmospheric leg as performed by previous studies (Dirmeyer, 2011; Dirmeyer et al., 2018). The strength of the atmospheric leg is quantified using the influence of daily SH on LCL defined as $\sigma(LCL) \cdot r(LCL, SH)$. The correlations between LCL and SH are expected to be positive since a shift of surface energy partitioning toward lower SH would result in cooler and wetter boundary layer and hence reduction in LCL. The LCL is calculated from instantaneous 3-D atmospheric variables that are saved for the last 4 years of simulations (2007 to 2010) from all experiments. The analysis of the atmospheric leg of coupling is therefore based on these 4 years of simulations.

3. Results

3.1. Model Skill During the Warm Season

Figures 3 and 4 show the biases in the climatology of warm season (April to August) precipitation and T-2 m in the model experiments with respect to NLDAS2 and PRISM. The common warm temperature and dry precipitation biases reported in global and regional simulations over the central United States (Klein et al., 2006; Lin et al., 2017) exist in our experiments as well. The April to August regional mean precipitation over the central United States is underestimated by 23% to 39%, and T-2 m is overestimated by 2.6 to 3.8 K in our numerical experiments. It is worth mentioning that model skill of precipitation and T-2 m over the central United States exhibits large sensitivity to changes in resolution and land use, consistent with the current understanding of regional climate over the region. As previously discussed, the warm season precipitation over the central United States is dominated by contribution from MCSs (Feng et al., 2016), the simulation of which are sensitive to model resolution (Prein, Liu, Ikeda, Trier, et al., 2017) and cloud microphysics parameterizations (Feng et al., 2018). The model skill in precipitation improves with finer resolution and more accurate land use representation (LU2000) over the central United States in our experiments.

Figures 3c–3h show the spatial pattern of biases in the climatology of warm-season (April to August) precipitation in all experiments with respect to NLDAS2 data. The precipitation skill over the central United States is dominated by the effect of atmospheric resolution. Simulations using the high-resolution land-atmosphere grid, LHAH, exhibit the lowest bias (regional mean bias of −23%). Figure 3b shows the variation in mean monthly bias and cRMSE of regional precipitation over the central United States with changing resolution and land use representation. The biases in precipitation are dependent on resolution and land use representation (range of 23% to 39%) while the interannual variability in monthly regional warm-season precipitation is similar in all experiments (not shown), as evidenced by the minor changes in the cRMSE (range of 29% to 34%). Experiments using the same land use, LU2000, show mean bias of −23% over the central United States in the LHAH experiments compared to the mean biases of −29% in the LHAL experiments and −36% in the LLAL experiments. At the same resolution, experiments using a more accurate land use (LU2000) show lower biases (Figure 3b). Therefore, resolution is the dominant factor influencing the warm season precipitation biases over the central United States in our model experiments, while the more accurate land representation plays a secondary role. Over the western and eastern United States, we note an overestimation of precipitation in the LHAH experiments (Figures S3a and S3b), primarily due to excess precipitation over mountainous areas with sharp terrain gradients of these regions.

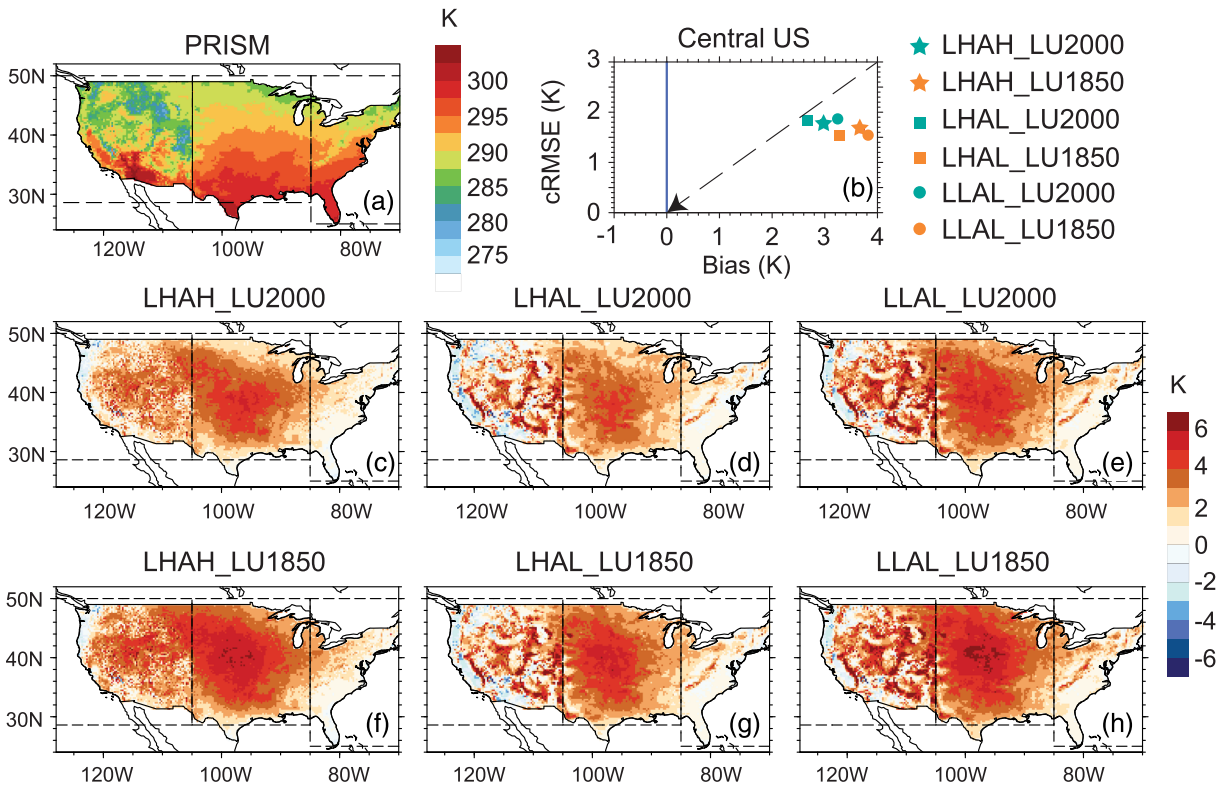

Figure 4. (a) Warm-season (AMJJA) 2-m air temperature (T-2 m, in K) for the period of 1984–2010 based on PRISM AMJJA; (b) regional T-2 m biases and RMSE over the central United States (in K). The arrow points toward increasing skill. (c–e) T-2 m biases in experiments using LU2000 at resolutions LHAH, LHAL, and LLAL, respectively (in K). (f–h) T-2 m biases in experiments using LU1850 at resolutions LHAH, LHAL, and LLAL, respectively (in K). The dashed lines show regions eastern, central, and western United States over which the regional errors statistics are calculated.

Figures 4c–4h show the spatial pattern of model biases in the climatology of warm-season (April to August) T-2 m in all experiments with respect to PRISM data. Figure 4b summarizes the mean monthly bias and cRMSE of regional T-2 m over the central United States. The mean warm temperature bias over the central United States ranges from 2.7 to 3.8 K. The model skill in mean seasonal cycle of T-2 m is largely unresponsive to resolution and land use representation, illustrated as similar cRMSEs in all experiments. The warm T-2 m bias is lower in simulations using the fine-resolution land grid (LHAL and LHAH) and more accurate land use representation (LU2000). The results indicate a significant influence of the land surface on model biases in T-2 m over the central United States, as the T-2 m bias is primarily dependent on land use representation. Experiments using the present-day land use (LU2000) on a fine-resolution land grid show lower T-2 m biases than similar experiments using the preindustrial land use (LU1850), irrespective of the atmosphere resolution (Figure 4b). Interestingly, we note the highest skill in T-2 m in the simulation using LU2000 on a fine-resolution land grid coupled to a coarse-resolution atmosphere grid (LHAL, regional mean bias of 2.7 K). The LHAH experiment exhibits a slightly higher regional mean bias of 3.0 K over the central United States, indicating that coupled land-atmospheric processes play a role in modulating warm-season T-2 m over the central United States. Over the western and eastern United States, the analysis does not show any specific pattern of variation in skill of T-2 m with changing resolution and land use representation (Figures S3c and S3d). Visually, over the mountainous terrain of western United States the fine-resolution LHAH experiments capture the spatial variations in T-2 m better (Figures 4c and 4f), similar to Huang et al. (2016).

Our CESM experiments show dry precipitation and warm T-2 m biases over the central United States, consistent with previously reported biases in regional and global simulations. The model biases in precipitation and T-2 m over the central United States are sensitive to both resolution and land use states. The precipitation biases over the central United States are primarily dependent on resolution rather than land use

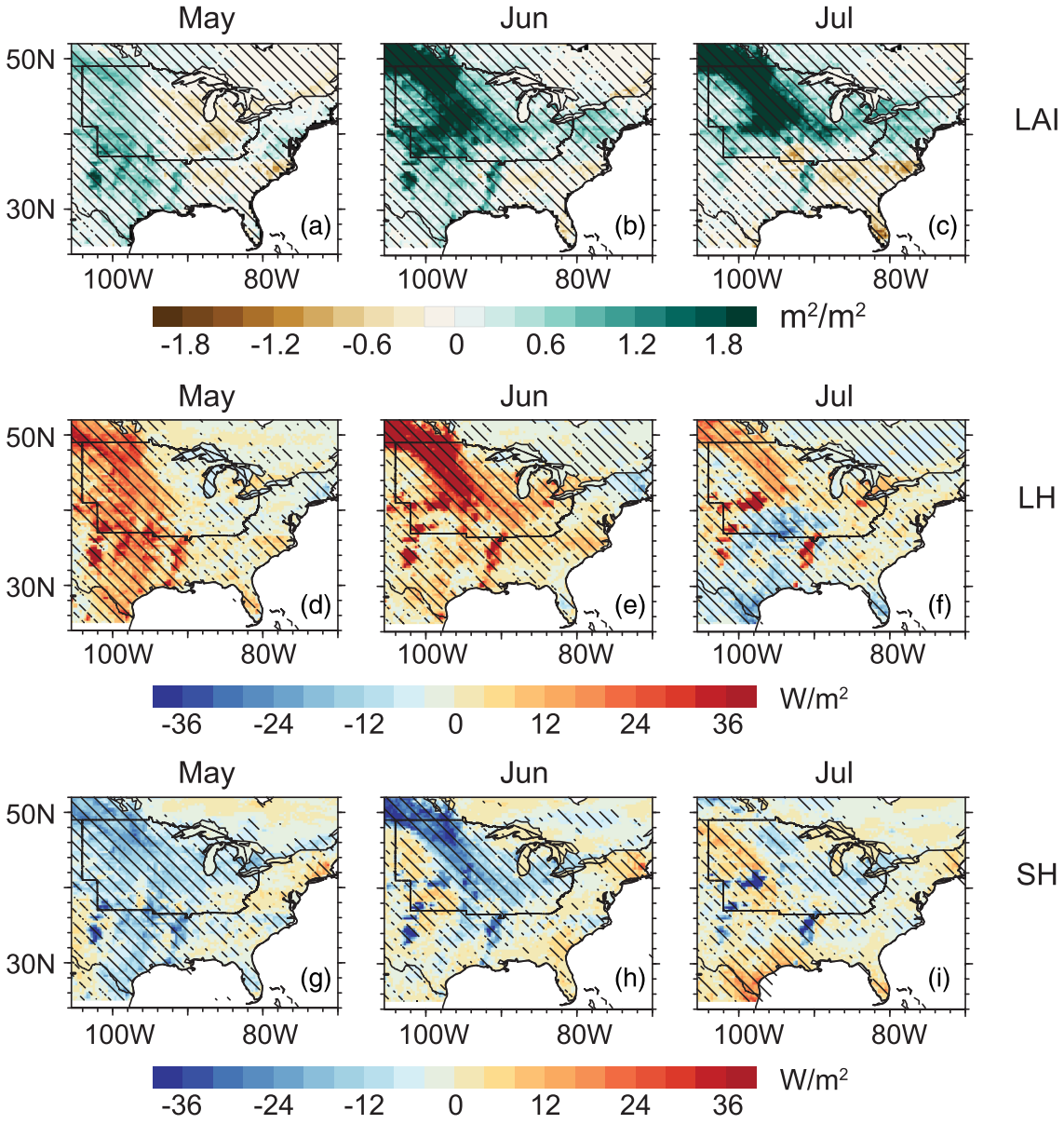

Figure 5. LULCC-induced changes (LU2000 minus LU1850) in LAI, LH, and SH in experiments at LHAH resolution during months May, June, and July of years 1984 to 2010. (a–c) LAI (in m^2/m^2). (d–f) LH (in W/m^2). (g–i) SH (in W/m^2). Hatching denotes statistically significant changes at 5% significance level.

representation. The LHAH simulation using the present-day land use (LU2000) exhibits the lowest biases in precipitation over this region. On the other hand, using accurate land use states that represent present-day is the most important factor influencing the model biases in T-2 m in our experiments. A fine-resolution land grid with more accurate land use representation coupled to a coarse-resolution atmosphere grid appears to be sufficient to attain a higher skill in T-2 m over this region. We will provide more discussions on this finding in the context of existing literature in section 4.

3.2. LULCC Impact on Near-Surface Climate of the Central United States

Here we present the LULCC-induced changes in near-surface climate of the central United States during the months May, June, and July, as these months correspond to the peak crop growing season in the model simulations and exhibit strongest LULCC effects.

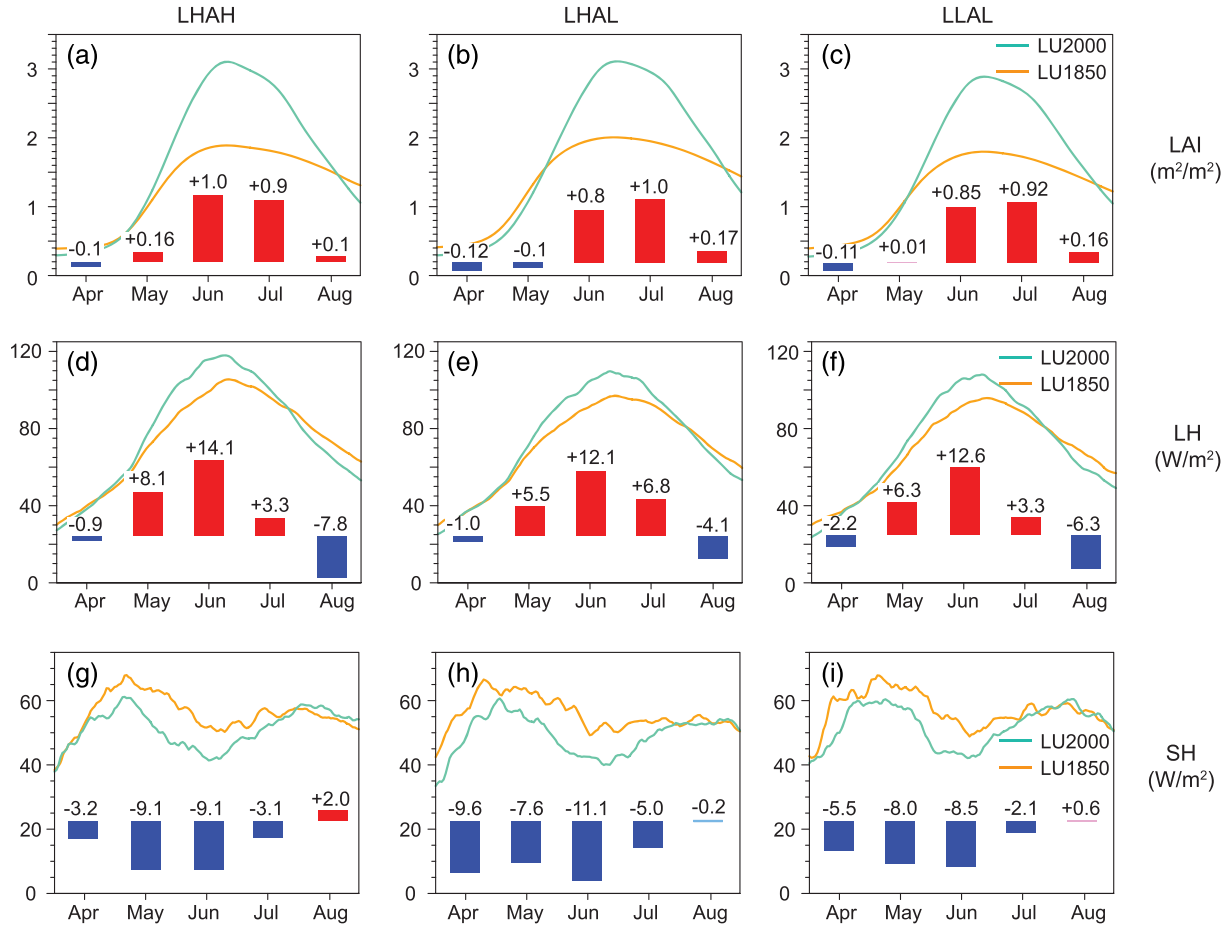

Figure 6. Warm-season (April to August) near-surface climate of Midwest in experiments at LHAH, LHAL, and LLAL resolutions (LU2000 versus LU1850). (a–c) LAI (in m^2/m^2). (d–f) LH (in W/m^2). (g–i) SH (in W/m^2). Month-wise changes are shown as bars in the panels (red bars indicate LU2000 minus LU1850 is positive and statistically significant at 5%, navy bars indicate LU2000 minus LU1850 is negative and statistically significant at 5%. The statistically insignificant positive and negative changes are shown as light pink and blue bars, respectively).

Figure 5 shows the LULCC-induced changes in LAI and surface latent (LH) and sensible (SH) heat fluxes in the LHAH experiments during the months May, June, and July. The changes in experiments at LHAL and LLAL resolutions are qualitatively similar (Figures S4 and S5). The conversion of natural vegetation (grassland and forests) to cropland over the central United States results in a positive change in LAI during the crop growing season from May to July. The strongest changes in LAI are over regions of grassland to cropland conversion. The Midwest (marked in Figures 1 and 5) is the region that has experienced the largest expansion of agriculture (Figure 1c). Consequently, the changes in LAI and surface fluxes are strongest in the Midwest. Broadly, the increase in LAI modifies the partitioning of energy at the land surface and results in an associated increase in latent heat fluxes and decrease in sensible heat flux.

Figure 6 shows the regional mean seasonal cycle of LAI and surface fluxes over the Midwest from all experiments, and the LULCC-induced significant changes are shown as bars in the panels. In the LHAH experiments, the surface fluxes show strong changes during both May (range 8 to 9 W/m^2) and June (range 9 to 14 W/m^2). Experiments using a coarser atmospheric resolution (LLAL and LHAL) exhibit strong changes during June (range 8.5 to 12.6 W/m^2), but the changes in surface fluxes during May are weaker (range 5.5 to 8 W/m^2) than in the high-resolution LHAH experiment.

We examine the associated changes in T-2 m and precipitation in Figures 7 and 8. The modified surface energy partitioning is associated with near-surface cooling and an increase in precipitation over the Midwest in May and June. These changes are consistent with observed trends in temperature and

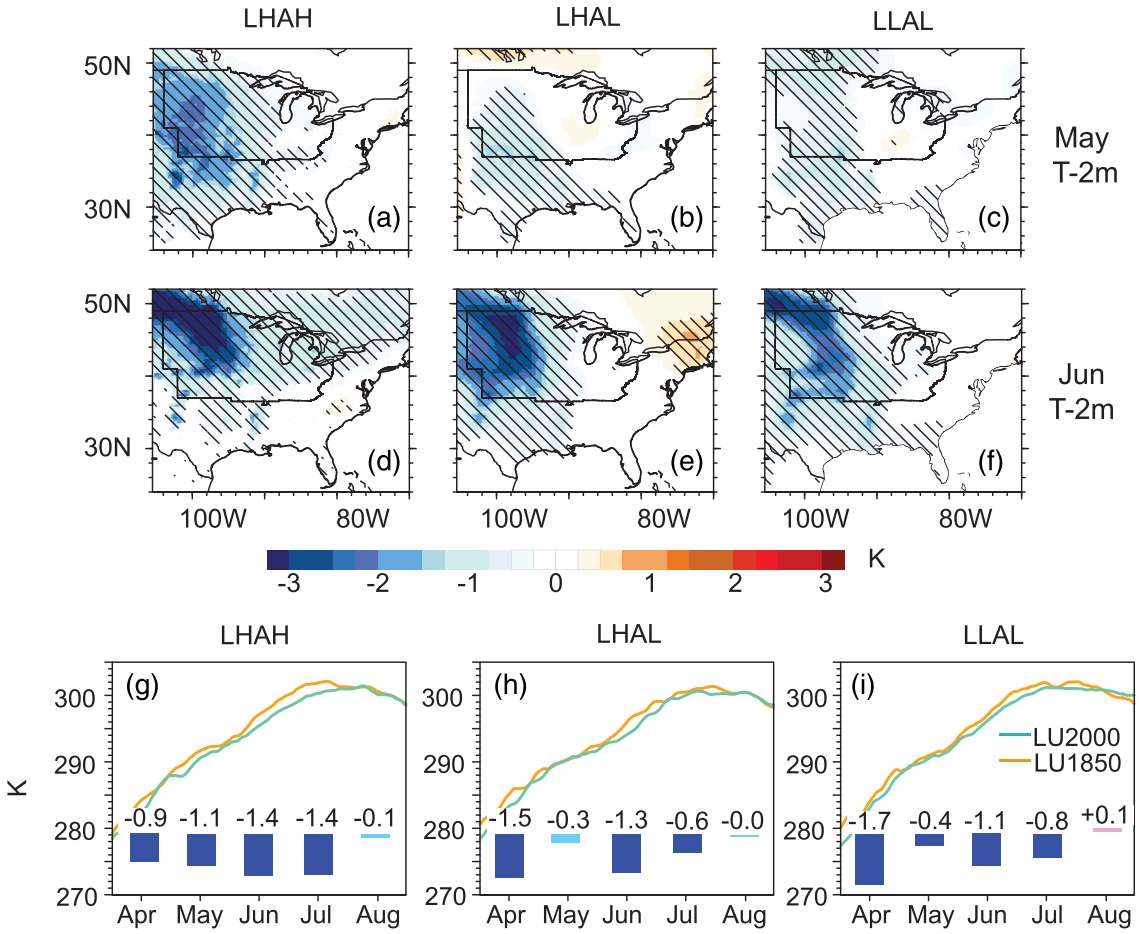

Figure 7. Changes in T-2 m in experiments at LHAH, LHAL, and LLAL resolutions. LULCC-induced changes (LU2000 minus LU1850) in T-2 m (in K) during (a–c) May and (d–f) June. Hatching denotes statistically significant changes at 5% significance level. (g–i) Warm season (April to August) T-2 m (in K) over Midwest (LU2000 versus LU1850). Month-wise changes are shown as bars in the panels (g)–(i) (navy bars indicate LU2000 minus LU1850 is negative and statistically significant at 5%. The statistically insignificant positive and negative changes are shown as light pink and blue bars, respectively).

precipitation over the Midwest (Alter et al., 2018; Andresen et al., 2012), reinforcing the existing consensus that historical LULCC have a strong influence on historical changes in climate of this region (Alter et al., 2018; Mueller et al., 2016).

Figure 7 shows the spatial pattern of LULCC-induced changes in T-2 m during May and June from all experiments and the seasonal cycle of the regional mean T-2 m over the Midwest. The significant changes in regional mean T-2 m are represented as bars in the panels. The spatial pattern of changes shows strongest cooling over areas of grass to crop conversion in the Midwest. The regional mean cooling of T-2 m over the Midwest ranges from 1.1 to 1.4 K in the LHAH experiment during the growing season from May to July. The LLAL and LHAL experiments show weaker cooling during these months. The changes are weakest during May in the LLAL and LHAL experiments, consistent with the weaker surface flux changes noted previously in Figure 6.

Figure 8 is similar to Figure 7, but for precipitation; the figure shows the spatial pattern of LULCC-induced changes in precipitation during May and June and the seasonal cycle of regional precipitation over the Midwest. The regional precipitation over the Midwest shows significant increases in the LHAH experiments during May (+0.33 mm day^{-1}) and June (+0.43 mm day^{-1}). During May, the LLAL and LHAL experiments do not exhibit any significant changes. These experiments show significant precipitation changes during June (+0.19 in LLAL and +0.32 mm day^{-1} in LHAL); however, the precipitation increases are lower in magnitude compared to that in the LHAH experiments.

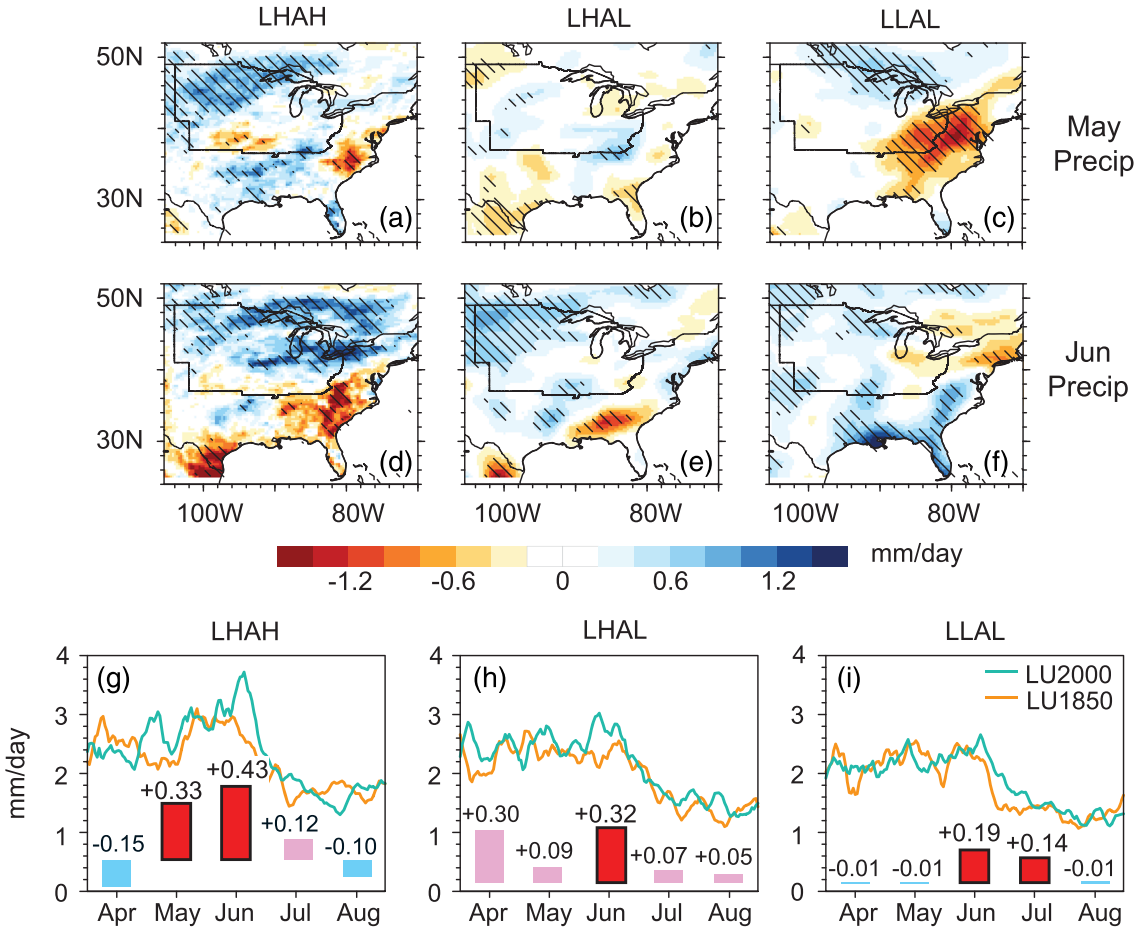

Figure 8. Changes in precipitation in experiments at LHAH, LHAL, and LLAL resolutions. LULCC-induced changes (LU2000 minus LU1850) in precipitation (in mm/day) during (a–c) May and (d–f) June. Hatching denotes statistically significant changes at 5% significance level . Month-wise changes in the warm season (April to August) are shown as bars in panels (g)–(i) (red bars indicate LU2000 minus LU1850 is positive and statistically significant at 5%. The statistically insignificant positive and negative changes are shown as light pink and blue bars, respectively).

3.3. LULCC Impact on MCS-Like Features Over Midwest

As discussed in section 3.2, LULCC from preindustrial to present-day results in significant increases in precipitation over the Midwest during May and June. Since MCSs contribute substantially to the spring and summer precipitation over the Midwest, we use hourly precipitation outputs for years 1999 to 2010 (12 years) to understand the LULCC impact on MCS-like features in the LHAH experiments and to evaluate their contribution to the precipitation increase discussed previously. The coarse atmosphere simulations (LHAL and LLAL) do not simulate trackable MCS features. We track MCS-like features in the LHAH experiments using the PF algorithm developed by Feng et al. (2016) as summarized in section 2.2.1. The number of MCS-like features over the Midwest in the LHAH simulations is close to that found in observations (Feng et al., 2016; Hu et al., 2020), particularly during May and June. However, the simulations largely underestimate the number of systems that initiate over the Midwest during the peak summer months of July and August. This underestimation is consistent with the modeled precipitation biases over the central United States discussed in section 3.1. The ranges of the mean rainfall intensity and mean PF area over the precipitation feature (PF, defined as contiguous area of grid-point rain rate >1 mm/hr) of the systems that initiate during May and June in the simulations are comparable to that in observations, even though the means are biased lower (Figure S6).

We examine the changes in MCS-like features due to LULCC in our experiments. Figure 9 shows the changes in total precipitation, MCS-like feature precipitation, and MCS-like feature counts on the CONUS

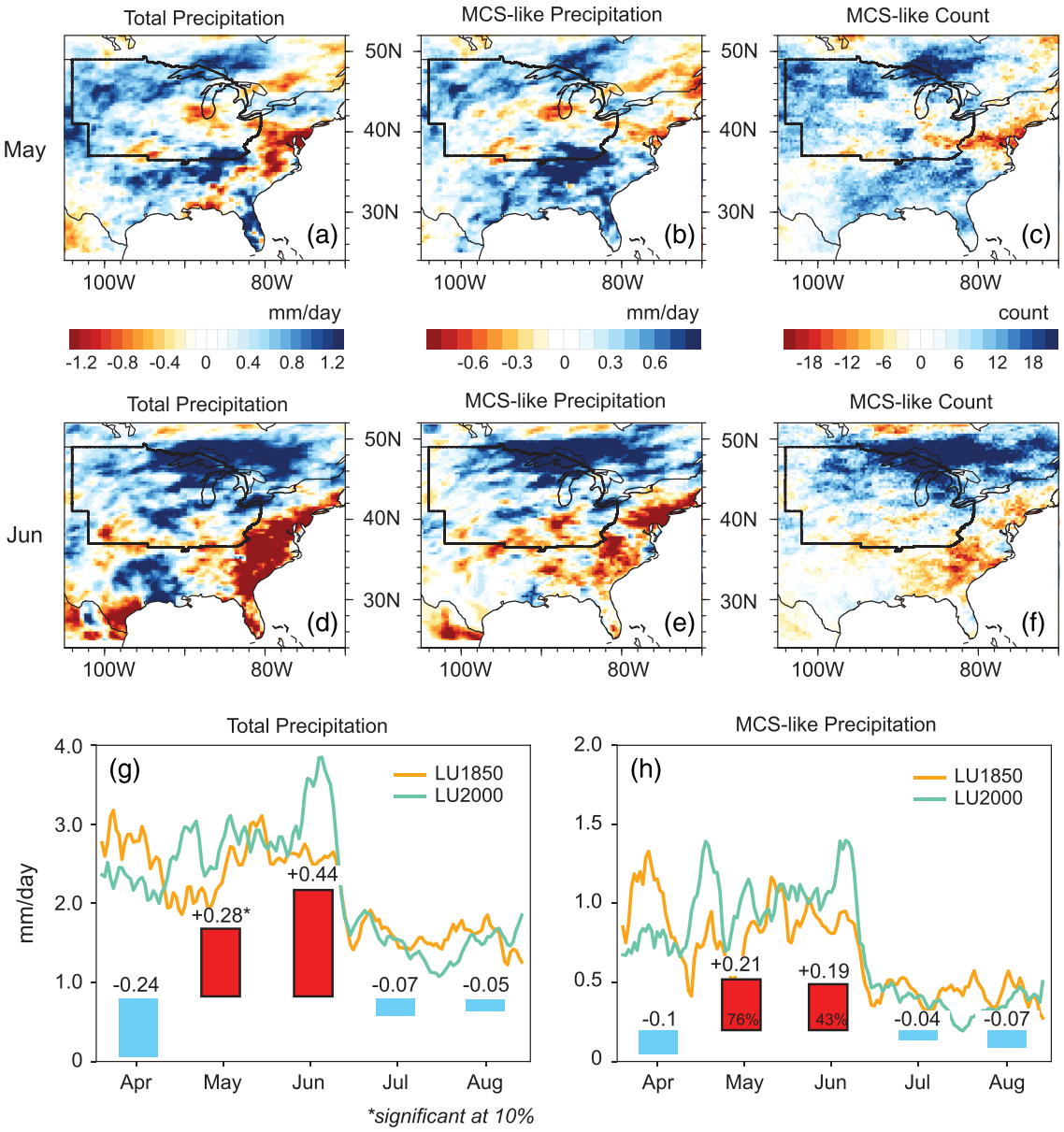

Figure 9. Spatial pattern of changes (LU2000 minus LU1850) in total precipitation (in mm/day), MCS-like precipitation (in mm/day), and MCS-like feature counts from experiments at LHAH resolution for years 1999 to 2010 (12 years) during (a–c) May and (d–f) June. Warm-season (April to August) precipitation (in mm/day) over the Midwest (LU2000 versus LU1850) (g) total precipitation and (h) MCS-like precipitation. Month-wise changes are shown as bars in the panels (g) and (h) (red bars indicate LU2000 minus LU1850 is positive and statistically significant at 5%. The statistically insignificant negative changes are shown as light blue bars).

grid from the LHAH experiments during May and June of years 1999 to 2010. During both months, the spatial pattern of changes in total precipitation, MCS-like precipitation, and MCS-like feature counts are similar (Figure 9a-f). Thus, the increase in MCS-like precipitation induced by LULCC contributes substantially to the increase in total precipitation in the LHAH experiments. The spatial similarity of changes in MCS-like feature precipitation and counts indicates that the increase in MCS-like precipitation comes from an increase in the number of MCS-like features over the Midwest. During May, the increase in MCS-like feature precipitation is due to an increase in the number of systems that occur over the Midwest. These MCS-like features do not show statistically significant changes in mean MCS PF area or the mean MCS rainfall intensity. During June, there is an increase in both the number of MCS-like

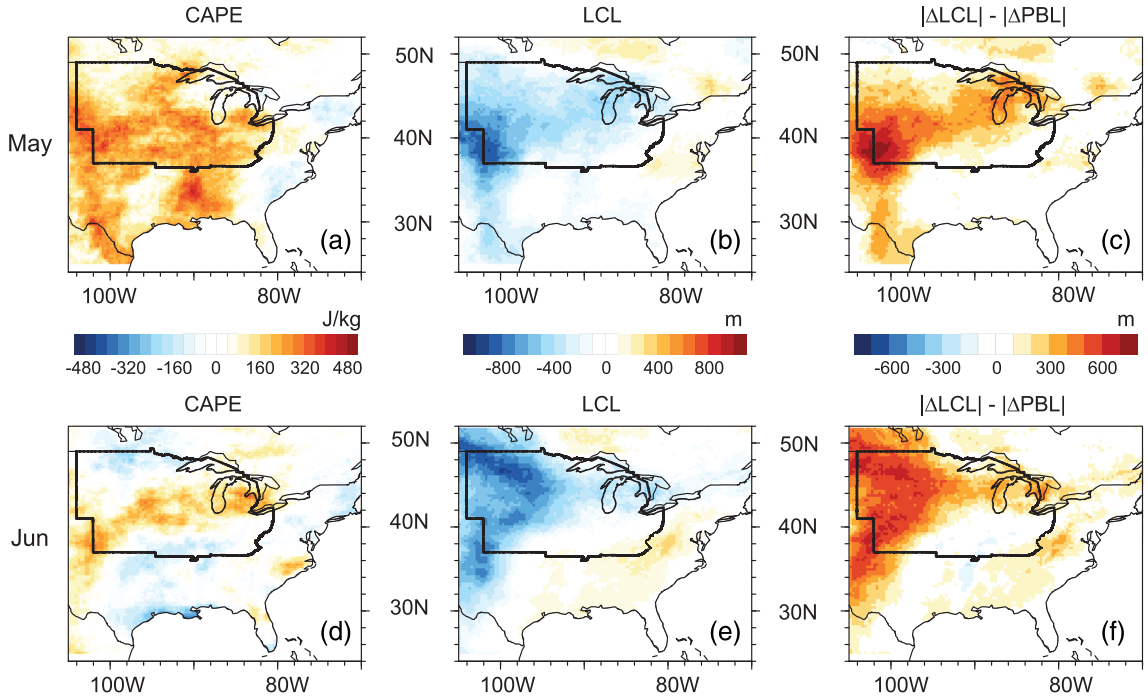

Figure 10. Spatial pattern of changes (LU2000 minus LU1850) in convective available potential energy (CAPE, in J/kg), lifted condensation level (LCL, in m), and the difference of absolute changes in lifted condensation level and planetary boundary layer height ($|\Delta LCL| - |\Delta PBL|$, in m) from experiments at LHAH resolution for years 2007 to 2010 (4 years) during (a–c) May and (d–f) June.

features and the mean rainfall intensity of these systems (Figure S6). Figures 9g and 9h show the regional mean seasonal cycle of total and MCS-like precipitation over Midwest in the LHAH experiments. During May, precipitation contributed by MCS-like features exhibits a statistically significant increase of +0.21 mm day^{-1} that accounts for 76% of the total precipitation change during this period (+0.28 mm day^{-1} during May of 1999 to 2010). The substantial contribution of the MCS-like precipitation to the total precipitation increase explains why the LLAL and LHAL experiments fail to capture the LULCC-induced precipitation increase in May, as coarse atmospheric resolution precludes these experiments from simulating such features. During June, the contribution of MCS-like precipitation to the total precipitation increase over the Midwest is relatively lower. MCS-like precipitation exhibits an increase of +0.19 mm day^{-1} in the LHAH experiments during June and accounts for 43% of the increase in total precipitation.

We use 6-hourly instantaneous outputs from the atmospheric model for years 2007 to 2010 to understand the changes in the thermodynamic environment over the Midwest associated with the increase in MCS-like precipitation in the LHAH experiments, similar to the analysis performed by (Qian et al., 2013). We examine the changes in convective available potential energy (CAPE, in J/kg), lifted condensation level (LCL, in m), and height of the planetary boundary layer (PBL, in m). Figures 10a and 10b and Figures 10d and 10e show the changes in mean daily CAPE and LCL during May and June in the LHAH experiments. The experiments show an increase in CAPE and reduction in LCL over the Midwest during May. During June, the increase in CAPE is weaker, but the LCL shows a larger decrease. The LULCC-induced decrease in sensible heat fluxes over the Midwest causes a near-surface cooling (section 3.2) and results in a reduction in the PBL as well. Figures 10c and 10f examine the change in LCL relative to the change in PBL and show the difference of the absolute changes in LCL and absolute changes in PBL ($|\Delta LCL| - |\Delta PBL|$). The reduction of LCL is larger than that of the PBL, indicating a higher probability of moist parcels to cross the LCL and hence more likely to form clouds and initiate surface-based convection. As a result, LULCC-induced changes in LCL and PBL are more favorable for potential MCS formation. Therefore, in these experiments, it appears that historical LULCC shifted the thermodynamic environment of the Midwest toward one that is more conducive for convection, particularly in May. During May, both CAPE and LCL show changes favorable

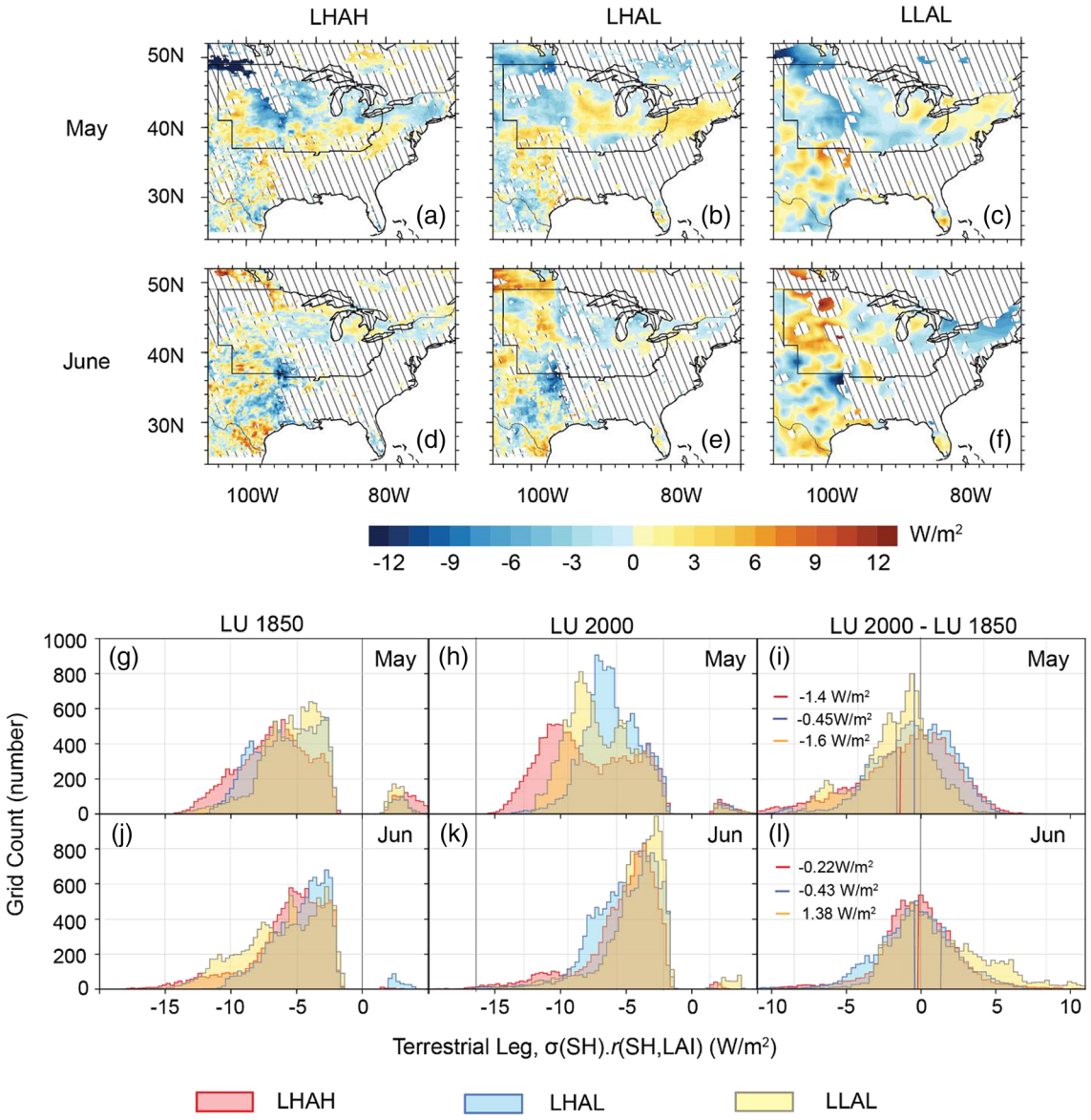

Figure 11. Spatial pattern LULCC-induced differences (LU2000 minus LU1850) in the strength of the terrestrial leg of land-atmosphere coupling between SH and LAI ($\sigma(SH)$. $r(LAI, SH)$, in W/m^2) in experiments at different resolutions during (a–c) May and (d–f) June. The areas masked out and hatched exhibit insignificant correlations between LAI and SH. Histograms of the mean and changes in the strength of the terrestrial leg over grids in Midwest during (g–i) May and (j–l) June.

for convection accounting for the stronger increase in MCS-induced precipitation. We note that besides local thermodynamic environments, different large-scale atmospheric environmental patterns also play a significant role in MCS initiation and MCS characteristics in the central United States (Feng et al., 2019; Song et al., 2019). Examination of the changes in atmospheric large-scale environments induced by LULCC is beyond the scope of this study, but such changes could have significant implications for regional climate and should be further investigated in future studies.

3.4. Changes in the Strength of Land-Atmospheric Coupling

In sections 3.2 and 3.3, we examine the changes in land and atmospheric variables induced by LULCC as the differences in the mean between simulations using LU2000 and LU1850. In this section, we investigate changes in the strength of coupling between land surface states, surface fluxes, and LCL to understand how changes in coupling strength influence the atmospheric response. Since the central United States is

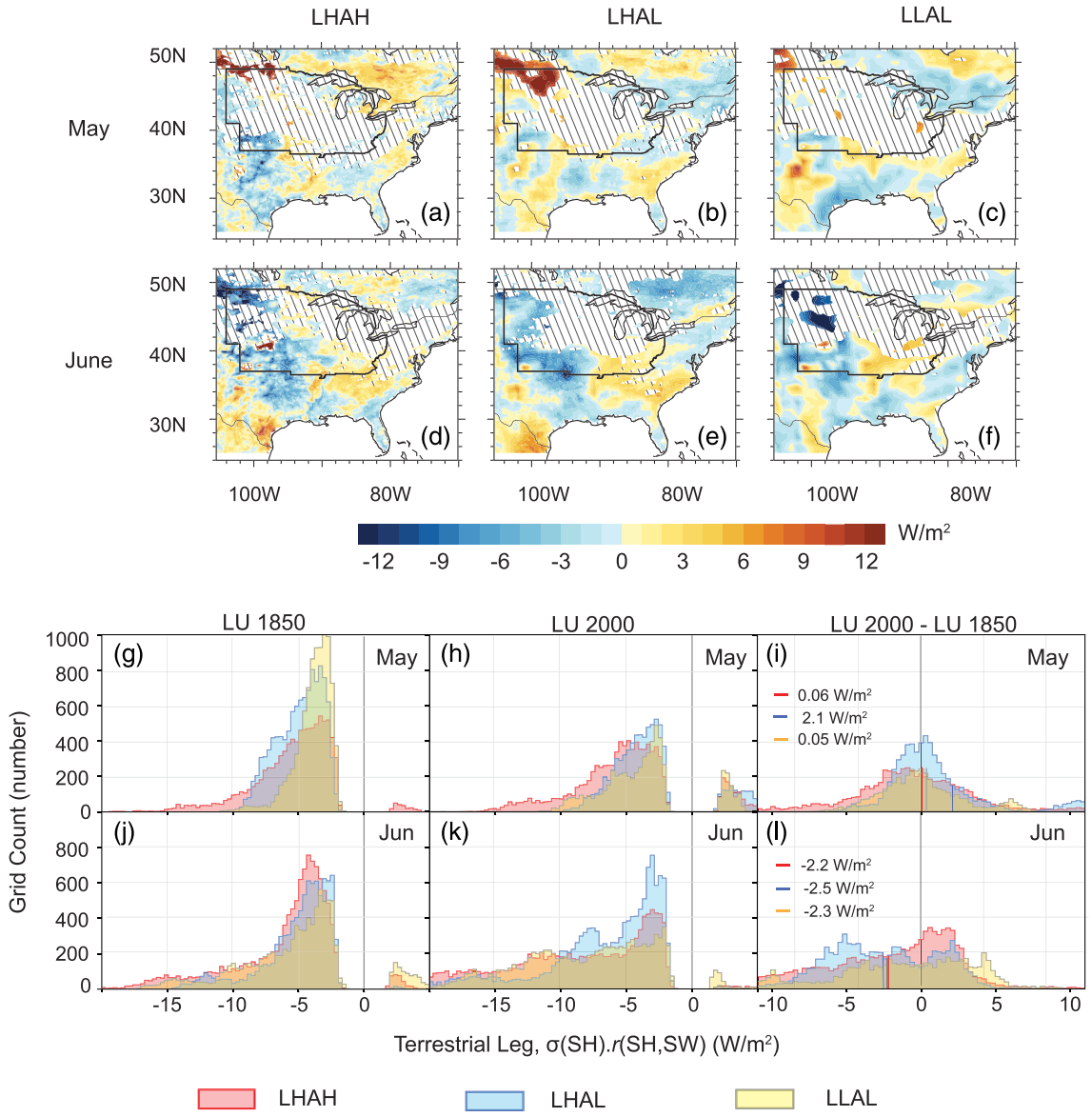

Figure 12. Spatial pattern LULCC-induced differences (LU2000 minus LU1850) in the strength of the terrestrial leg of land-atmosphere coupling between SH and SW ($\sigma(SH)$. $r(SW, SH)$, in W/m^2) in experiments at different resolutions during (a–c) May and (d–f) June. The areas masked out and hatched exhibit insignificant correlations between LAI and SW. Histograms of the mean and changes in the strength of the terrestrial leg over grids in Midwest during (g–i) May and (j–l) June.

understood to be a hotspot of land-atmosphere coupling (Koster et al., 2004), changes in coupling strength may affect the model response to LULCC. We focus on the coupling strength during the months of May and June, in which LULCC-induced changes in the thermodynamic environment over the Midwest is evident. During May and June, there is an increase in vegetation and near-surface temperature with a seasonal progression toward summer (Figure 6 and Figures 7g–7i). There are associated changes in soil water, surface fluxes, and near-surface atmospheric moisture in the coupled land-atmosphere system in both LU2000 and LU1850 simulations (Figure S7).

Here we examine the changes in the strength of land-atmosphere coupling to understand how it influences the changes in atmospheric states in our experiments. The analysis presented here focuses on the difference in the strength of coupling between land and atmosphere in the model experiments at different resolutions. Statistical coupling indices detailed in section 2.2.2 are used to quantify the strength of the terrestrial and atmospheric legs of coupling. The indices describe (1) the sensitivity of surface flux (SH) to changes in

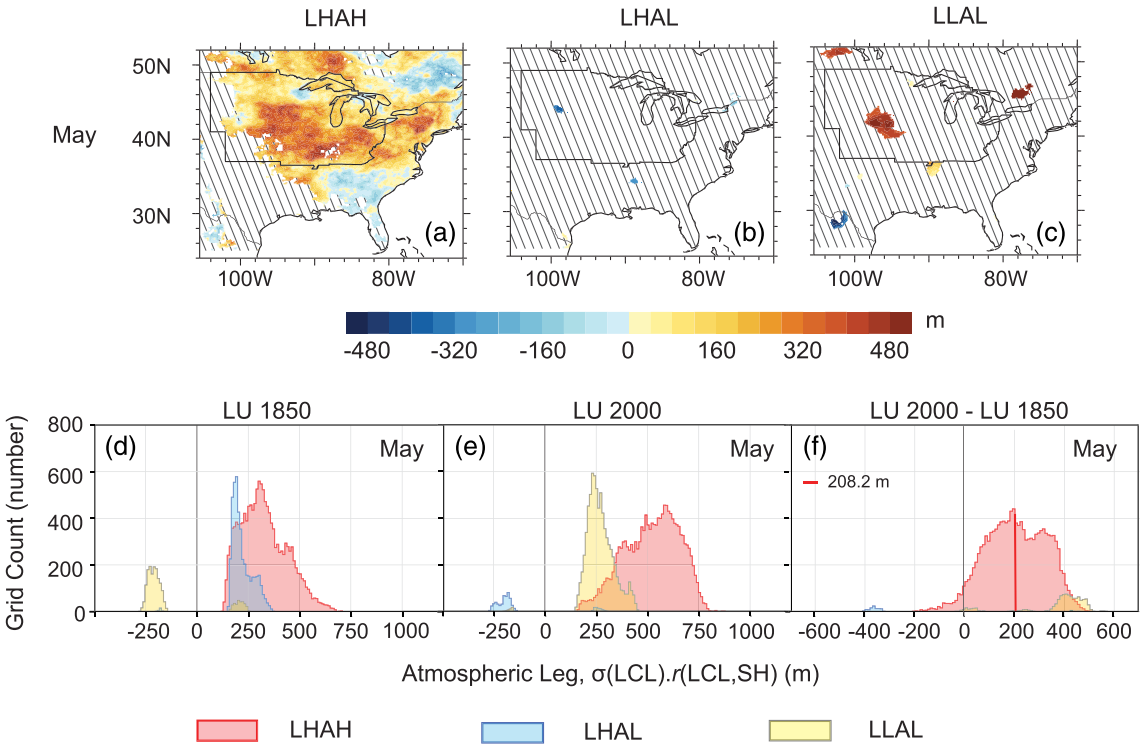

Figure 13. (a–c) Spatial patterns of LULCC-induced differences (LU2000 minus LU1850) in the strength of atmospheric-leg LA coupling in the ($\sigma(LCL)$. $r(LCL, SH)$, in m) in experiments at different resolutions in May. The areas masked out and hatched exhibit insignificant correlations between SH and LCL. (d–f) Histograms of the mean and changes in the strength of the atmospheric-leg LA coupling over the Midwest in May. In the LHAH and LLAL experiments, majority of the grid points do not exhibit a significant SH-LCL association.

land state variables (LAI and SW) and (2) the sensitivity of LCL to changes in surface flux (SH). The purpose of this analysis is to understand how land-atmosphere coupling strength changes with resolution and land use in our experiments and the effect of changes in coupling strength on the atmospheric states. The influence of changes in land surface on temperature and precipitation is more complex (Chen & Dirmeyer, 2016) and cannot be inferred directly from this analysis of coupling strength.

Figures 11a–11f and Figures 12a–12f show the spatial patterns of the differences in the strength of the terrestrial leg of coupling during May and June in all three experiments. During May, LULCC intensifies the LAI-SH coupling, mainly over areas of grass to crop conversion in the Midwest in all sets of experiments. The grids do not exhibit strong SW-SH coupling during May. During June, the LAI-SH coupling strength in the Midwest exhibits a mix of weaker changes; but there are some areas in the Midwest that exhibit stronger changes in the SW-SH coupling strength. The changes in the strength of the terrestrial leg of coupling is summarized using histograms in Figures 11g–11l and Figures 12g–12l. The histograms show distributions of indices of the terrestrial leg in the LU2000 and LU1850 experiments and the changes in coupling strength induced by LULCC over the Midwest. These histograms are comparable since all experiments have been interpolated to the NLDAS grid and have equal number of grid cells in the Midwest. The spatial distribution of the strength of the terrestrial leg is similar in experiments at three different resolutions, as evidenced by the overlap of histograms in Figures 11g and 11h and Figures 11j and 11k. The LHAH experiment using LU2000 exhibits a slightly stronger LAI-SH coupling strength than the other two experiments in May (Figure 11h). Figures 11i and 11l show the impact of LULCC on the terrestrial leg coupling strength as the difference between the LU2000 and LU1850 experiments. During May, LULCC leads to strengthening of the LAI-SH coupling over parts of the Midwest by 0.45 to 1.4 W/m^2 (9% to 33% from LU1850 mean coupling strength) (Figure 11i). During June, the analysis reveals a strengthening of the SW-SH coupling by 2.2 to 2.5 W/m^2 (36% to 50%) over parts of the Midwest (Figure 12l). Therefore, overall, we note a LULCC-induced strengthening of the terrestrial leg of land-atmosphere coupling in the experiments at all three resolutions.

Similar to Figures 11 and 12, Figure 13 shows the strength of the atmospheric leg of coupling during May in all three experiments. During June, the index is not calculated because the correlations between SH and LCL are not significant over most of the grid cells. The atmospheric leg of coupling shows strong changes during May only in the LHAH experiments, while the correlations between SH and LCL are insignificant in the other two experiments (areas masked out and hatched in Figures 12a–12c). The spatial patterns of difference between the simulations (LU2000 minus LU1850) show that the strength of the atmospheric leg of coupling is intensified over the Midwest, signifying a stronger response of LCL to changes in surface SH in the LHAH experiments. The histograms of the strength of SH-LCL coupling (Figures 12d and 12e) illustrate that both LHAH simulations (LU1850 and LU2000) show stronger coupling in the atmospheric leg in May compared to simulations using a coarse atmospheric resolution. LULCC strengthens the atmospheric leg in this experiment by 208.2 m (64% from LU1850 mean coupling strength) (Figure 12f).

The strengthening of the atmospheric leg of coupling in May shown in Figure 12 is primarily due to the increase in the sensitivity of LCL to changes in SH ($\frac{dLCL}{dSH}$) (Figure S8). The shift in surface energy partitioning toward reduced SH is hence associated with a strong reduction in LCL. The LULCC-induced increase in the intensity of SH-LCL coupling in the LHAH experiments contributes to the lowering of LCL over the Midwest in May noted in section 3.3. The reduced SH and the increased sensitivity of LCL to SH in the LHAH_LU2000 experiment results in a strong reduction of LCL over the Midwest in May. This leads to a higher probability of convective initiation over the Midwest and a subsequent increase in the precipitation from MCS-like features induced by LULCC.

4. Summary and Conclusions

We performed historical simulations using uniform and VR configurations of CESM2, employing three different land-atmosphere grid combinations. The experiments are designed to study the impact of LULCC on the warm-season regional climate of the central United States and the resolution dependence of the simulated impacts. We also study the influence of resolution and land use states on the model skill for precipitation and T-2 m over the central United States. Our analysis reveals that model skill is sensitive to both resolution and land use states. The model skill in simulating precipitation over the central United States is primarily influenced by atmosphere resolution. That is, the VR model configurations using fine-resolution atmosphere grid coupled to fine-resolution land grid exhibit the lowest error statistics for precipitation. The reduction of precipitation bias in the VR LHAH experiment is associated with reduced T-2 m bias compared to the coarse-resolution LLAL experiments. However, land use representation is the dominant factor influencing the model skill in simulating T-2 m in the central United States. Use of a fine-resolution land grid with accurate land use representation is sufficient to attain higher model skill in T-2 m. An additional simulation employing a high resolution atmosphere coupled to a low-resolution land grid (LLAH) would help substantiate the influence of land and atmosphere resolution on model skill. However, the computational cost of such an experiment is similar to the LHAH experiment since the atmospheric component accounts for more than 90% of the computational cost of a typical land-atmosphere CESM simulation. Hence, we have not included an LHAH experiment here due to computational constraints.

We note that the biases in our experiments are consistent with the current understanding from literature. Recent literature document multimodel experiments at resolutions of 30 to 300 km to understand the warm season temperature biases in the central United States (Morcrette et al., 2018; Van Weverberg et al., 2018) as part of the "Clouds Above the Unites States and Errors at the Surface" (CAUSES) project. The results of the CAUSES project indicate that the dominant reasons behind the biases vary among the models and are linked to two main factors. One factor is the deficiencies in surface energy partitioning which is influenced by the representation of the land surface and the input of precipitation to the land surface (Ma et al., 2018; Zhang et al., 2018). The precipitation bias itself is primarily associated with deficiencies in major precipitation events (Klein et al., 2006; Lin et al., 2017). The other factor is convective cloudiness, which is determined by the radiative properties of clouds, their interactions with shortwave radiation, and other atmospheric parameterizations that influence the occurrence of convective cloud types (Morcrette et al., 2018; Van Weverberg et al., 2018).

Therefore, the current understanding indicates that model biases in the central United States are associated with both the representation of land and atmosphere processes and the model horizontal resolution, consistent with the biases reported here. The interactions between these processes that influence the model biases are not fully understood yet (Feng et al., 2019; Song et al., 2019). Future research on both model resolution and improving physics parameterizations are required to understand and alleviate the model biases.

We analyze the impacts of LULCC over the central United States using the experiments. Historical LULCC from preindustrial to present-day drives an increase in LAI over the Midwest during the peak crop growing season from May to July. The higher LAI is associated with change in surface energy partitioning resulting in an increase in surface LH and decrease in surface SH. We note that LULCC induces a significant near-surface cooling over the Midwest along with increases in warm season precipitation. These changes are consistent with reported historical trends in precipitation and temperature in this region (Andresen et al., 2012; Grotjahn & Huynh, 2018). The cooling of summer temperatures over the Midwest is potentially influenced by changes in global SSTs (Meehl et al., 2012; Partridge et al., 2018), regional aerosols (Leibensperger et al., 2012; Portmann et al., 2009), and vegetation changes (Alter et al., 2018; Mueller et al., 2016). LULCC-induced near-surface cooling over the central United States is also reported by previously published model and observation-based studies (Diffenbaugh, 2009; Fall et al., 2010; Ge, 2010). Our experiments show stronger cooling in the high-resolution experiment compared to experiments using a coarse atmospheric resolution. The mean magnitudes of cooling over the Midwest are 1.1 to 1.4 K during May to July in the high-resolution (LHAH) experiments.

The high-resolution experiments exhibit significant increases in precipitation over the Midwest in May and June. The changes in precipitation are weaker/insignificant in experiments using a coarse atmospheric resolution. MCS-like precipitation contributes substantially (76%) to the LULCC-induced increase in precipitation over the Midwest in May. This change in MCS-like precipitation appears to be caused by an increase in the number of MCS-like features that is driven by the change from preindustrial to present-day land use. Historical LULCC shifts the thermodynamic environment of the Midwest toward one that is more conducive for convection. In the high-resolution experiments, LULCC strengthens the atmospheric leg of land-atmosphere coupling, heightening the sensitivity of LCL to changes in surface SH and contributing to the lowering of the LCL.

Due to computational and storage constraints, we were unable to conduct ensemble simulations to explore the uncertainty bounds of the findings documented. However, the experiments and analysis presented here demonstrate the potential of using VR-ESMs for hydroclimatic simulations in regions of major LULCC. The LULCC effects on thermodynamic environment and MCS-like features over the Midwest reported here have important implications. Observations in the past 35 years document an increase in frequency and intensity of MCS precipitation over the central United States (Feng et al., 2016). A previous modeling study reports that the intensity of MCSs and hence the precipitation volume from these systems are expected to increase in a future climate (Prein, Liu, Ikeda, Bullock, et al., 2017). Our analyses of high-resolution simulations indicate that the increase in frequency of these systems is potentially also a function of LULCC in the region, especially during the spring to summer transition months. There could be potential effects on these systems during the late summer months as well, which are missing in our experiments due to the typically lower skill of ESMs in simulating these late summer systems (Feng et al., 2019). Further studies that address the uncertainty in these reported effects and potential effects on MCSs during late summer are thus necessary to better characterize the observed and expected future changes in these systems due to historic and future LULCC.

Data Availability Statement

The namelist settings and driving scripts used to perform the CESM2 experiments are available at 10.5281/zenodo.3799314. The CESM model outputs generated for these experiments have been made available at https://portal.nersc.gov/archive/home/d/devanand/www/LULCC_CESMVR_Experiments. NLDAS2 data used in this study were acquired as part of the mission of NASA's Earth Science Division and archived and distributed by the Goddard Earth Sciences (GES) Data and Information Services Center (DISC). PRISM data used in this study are acquired from the PRISM Climate Group, Oregon State University, http://prism.oregonstate.edu, created 4 February 2004.

Acknowledgments

A.D., M.H., Z.F., Y.Q., and Z.Y. were supported by the U.S. Department of Energy (DOE), Office of Science, as part of research in Multi-Sector Dynamics, Earth and Environmental System Modeling Program. D.M.L. is supported by the National Center for Atmospheric Research, which is a major facility sponsored by the National Science Foundation (NSF) under Cooperative Agreement No. 1852977. D.M.L. was also supported in part by the RUBISCO Scientific Focus Area (SFA), which is sponsored by the Regional and Global Climate Modeling (RGCM) Program in the Climate and Environmental Sciences Division (CESD) of the Office of Biological and Environmental Research in the U.S. Department of Energy Office of Science and by National Institute of Food and Agriculture/U.S. Department of Agriculture Grant 2015-67003-23485. The authors would like to acknowledge Drs. Sean Swenson and Keith Oleson for their advice and assistance in model configurations at the initial stage of this study.

References

Alter, R. E., Douglas, H. C., Winter, J. M., & Eltahir, E. A. B. (2018). Twentieth century regional climate change during the summer in the central United States attributed to agricultural intensification. *Geophysical Research Letters*, *45*, 1586–1594. https://doi.org/10.1002/2017GL075604

Andresen, J., Hilberg, S., Kunkel, K., Winkler, J., Andresen, J., Hatfield, J., et al. (2012). *Historical climate and climate trends in the Midwestern USA National Climate Assessment Midwest Technical Input Report*, Ann Arbor, MI, USA and Ames, IA, USA: Great Lakes Integrated Sciences and Assessments Center and National Laboratory for Agriculture and the Environment. Retrieved from http://glisa.msu.edu/docs/NCA/MTIT_Historical.pdf

Bogenschutz, P. A., Gettelman, A., Morrison, H., Larson, V. E., Craig, C., & Schanen, D. P. (2013). Higher-order turbulence closure and its impact on climate simulations in the Community Atmosphere Model. *Journal of Climate*, *26*(23), 9655–9676. https://doi.org/10.1175/JCLI-D-13-00075.1

Brovkin, V., Boysen, L., Arora, V. K., Boisier, J. P., Cadule, P., Chini, L., et al. (2013). Effect of anthropogenic land-use and land-cover changes on climate and land carbon storage in CMIP5 projections for the twenty-first century. *Journal of Climate*, *26*(18), 6859–6881. https://doi.org/10.1175/JCLI-D-12-00623.1

Butler, E. E., Mueller, N. D., & Huybers, P. (2018). Peculiarly pleasant weather for US maize. *Proceedings of the National Academy of Sciences of the United States of America*, *115*(47), 11935–11940. https://doi.org/10.1073/pnas.1808035115

Cheinet, S., Beljaars, A., Morcrette, J.-J., & Viterbo, P. (2005). *Assessing physical processes in the ECMWF model forecasts using the ARM SGP observations*. Reading, UK: European Centre for Medium-range Weather Forecasts.

Chen, L., & Dirmeyer, P. A. (2016). Adapting observationally based metrics of biogeophysical feedbacks from land cover/land use change to climate modeling. *Environmental Research Letters*, *11*(3). https://doi.org/10.1088/1748-9326/11/3/034002

Chen, L., Dirmeyer, P. A., Chen, L., & Dirmeyer, P. A. (2017). Impacts of land-use/land-cover change on afternoon precipitation over North America. *Journal of Climate*, *30*(6), 2121–2140. https://doi.org/10.1175/JCLI-D-16-0589.1

Cheruy, F., Dufresne, J. L., Hourdin, F., & Ducharne, A. (2014). Role of clouds and land-atmosphere coupling in midlatitude continental summer warm biases and climate change amplification in CMIP5 simulations. *Geophysical Research Letters*, *41*, 6493–6500. https://doi.org/10.1002/2014GL061145

Davin, E. L., & de Noblet-Ducoudré, N. (2010). Climatic impact of global-scale deforestation: Radiative versus nonradiative processes. *Journal of Climate*, *23*(1), 97–112. https://doi.org/10.1175/2009JCLI3102.1

de Noblet-Ducoudré, N., Boisier, J.-P., Pitman, A., Bonan, G. B., Brovkin, V., Cruz, F., et al. (2012). Determining robust impacts of land-use-induced land cover changes on surface climate over North America and Eurasia: Results from the first set of LUCID experiments. *Journal of Climate*, *25*(9), 3261–3281. https://doi.org/10.1175/JCLI-D-11-00338.1

Diffenbaugh, N. S. (2009). Influence of modern land cover on the climate of the United States. *Climate Dynamics*, *33*(7–8), 945–958. https://doi.org/10.1007/s00382-009-0566-z

Diffenbaugh, N. S., Ashfaq, M., & Scherer, M. (2011). Transient regional climate change: Analysis of the summer climate response in a high-resolution, century-scale ensemble experiment over the continental United States. *Journal of Geophysical Research*, *116*(D24). https://doi.org/10.1029/2011JD016458

Dirmeyer, P. A. (2011). The terrestrial segment of soil moisture-climate coupling. *Geophysical Research Letters*, *38*, L16702. https://doi.org/10.1029/2011GL048268

Dirmeyer, P. A., Chen, L., Wu, J., Shin, C.-S., Huang, B., Cash, B. A., et al. (2018). Verification of land-atmosphere coupling in forecast models, reanalyses, and land surface models using flux site observations. *Journal of Hydrometeorology*, *19*(2), 375–392. https://doi.org/10.1175/JHM-D-17-0152.1

Fall, S., Niyogi, D., Gluhovsky, A., Pielke, R. A., Kalnay, E., & Rochon, G. (2010). Impacts of land use land cover on temperature trends over the continental United States: Assessment using the North American Regional Reanalysis. *International Journal of Climatology*, *30*(13), 1980–1993. https://doi.org/10.1002/joc.1996

Fan, J., Han, B., Varble, A., Morrison, H., North, K., Kollias, P., et al. (2017). Cloud-resolving model intercomparison of an MC3E squall line case: Part I—Convective updrafts. *Journal of Geophysical Research: Atmospheres*, *122*, 9351–9378. https://doi.org/10.1002/2017JD026622

Feddema, J. J., Oleson, K. W., Bonan, G. B., Mearns, L. O., Buja, L. E., Meehl, G. A., & Washington, W. M. (2005). The importance of land-cover change in simulating future climates. *Science (New York, N.Y.)*, *310*(5754). https://doi.org/10.1126/science.1118160

Feng, Z., Houze, R. A., Leung, L. R., Song, F., Hardin, J. C., Wang, J., et al. (2019). Spatiotemporal characteristics and large-scale environments of mesoscale convective systems east of the Rocky Mountains. *Journal of Climate*, *32*. https://doi.org/10.1175/JCLI-D-19-0137.1

Feng, Z., Leung, L. R., Hagos, S., Houze, R. A., Burleyson, C. D., & Balaguru, K. (2016). More frequent intense and long-lived storms dominate the springtime trend in central US rainfall. *Nature Communications*, *7*(1). https://doi.org/10.1038/ncomms13429

Feng, Z., Leung, L. R., Houze, R. A., Hagos, S., Hardin, J., Yang, Q., et al. (2018). Structure and evolution of mesoscale convective systems: Sensitivity to cloud microphysics in convection-permitting simulations over the United States. *Journal of Advances in Modeling Earth Systems*, *10*(7), 1470–1494. https://doi.org/10.1029/2018MS001305

Findell, K. L., Berg, A., Gentine, P., Krasting, J. P., Lintner, B. R., Malyshev, S., et al. (2017). The impact of anthropogenic land use and land cover change on regional climate extremes. *Nature Communications*, *8*(1). https://doi.org/10.1038/s41467-017-01038-w

Gates, W. L., Boyle, J. S., Covey, C., Dease, C. G., Doutriaux, C. M., Drach, R. S., et al. (1999). An overview of the results of the Atmospheric Model Intercomparison Project (AMIP I). *Bulletin of the American Meteorological Society*, *80*. https://doi.org/10.1175/1520-0477(1999)080<0029:AOOTRO>2.0.CO;2

Ge, J. (2010). MODIS observed impacts of intensive agriculture on surface temperature in the southern Great Plains. *International Journal of Climatology*, *30*(13), 1994–2003. https://doi.org/10.1002/joc.2093

Gettelman, A., Callaghan, P., Larson, V. E., Zarzycki, C. M., Bacmeister, J. T., Lauritzen, P. H., et al. (2018). Regional climate simulations with the Community Earth System Model. *Journal of Advances in Modeling Earth Systems*, *10*(6), 1245–1265. https://doi.org/10.1002/2017MS001227

Gettelman, A., & Morrison, H. (2015). Advanced two-moment bulk microphysics for global models. Part I: Off-line tests and comparison with other schemes. *Journal of Climate*, *28*(3), 1268–1287. https://doi.org/10.1175/JCLI-D-14-00102.1

Golaz, J.-C., Larson, V. E., Cotton, W. R., Golaz, J.-C., Larson, V. E., & Cotton, W. R. (2002). A PDF-Based Model for Boundary Layer Clouds. Part I: Method and Model Description. *Journal of the Atmospheric Sciences*, *59*(24), 3540–3551. https://doi.org/10.1175/1520-0469(2002)059<3540:APBMFB>2.0.CO;2

Grotjahn, R., & Huynh, J. (2018). Contiguous US summer maximum temperature and heat stress trends in CRU and NOAA Climate Division data plus comparisons to reanalyses. *Scientific Reports*, *8*(1). https://doi.org/10.1038/s41598-018-29286-w

Hibbard, K., Hoffman, F. M., Huntzinger, D., & West, T. O. (2017). Changes in land cover and terrestrial biogeochemistry. In D. J. Wuebbles, D. W. Fahey, K. A. Hibbard, D. J. Dokken, B. C. Stewart, & T. K. Maycock (Eds.), *Climate Science Special Report: Fourth National Climate Assessment* (Chap. 10, Vol. I, pp. 277–302). Washington, DC: U.S. Global Change Research Program. https://doi.org/10.7930/J0416V6X

Hu, H., Leung, L. R., & Feng, Z. (2020). Observed warm-season characteristics of MCS and non-MCS rainfall and their recent changes in the central United States. *Geophysical Research Letters*, *47*, e2019GL086783. https://doi.org/10.1029/2019GL086783

Huang, X., Rhoades, A. M., Ullrich, P. A., & Zarzycki, C. M. (2016). An evaluation of the variable-resolution CESM for modeling California's climate. *Journal of Advances in Modeling Earth Systems*, *8*(1), 345–369. https://doi.org/10.1002/2015MS000559

Hurtt, G. C., Chini, L. P., Sahajpal, R., Frolking, S. E., Bodirsky, B., Calvin, K. V., et al. (2018). LUH2: Harmonization of global land-use scenarios for the period 850-2100. In *American Geophysical Union, Fall Meeting 2018, Abstract #GC13A-01 GC13A-01*, Washington, D.C., USA: American Geophysical Union. Retrieved from http://adsabs.harvard.edu/abs/2018AGUFMGC13A..01H

Jiang, X., Lau, N.-C., & Klein, S. A. (2006). Role of eastward propagating convection systems in the diurnal cycle and seasonal mean of summertime rainfall over the U.S. Great Plains. *Geophysical Research Letters*, *33*, L19809. https://doi.org/10.1029/2006GL027022

Klein, S. A., Jiang, X., Boyle, J., Malyshev, S., & Xie, S. (2006). Diagnosis of the summertime warm and dry bias over the U.S. Southern Great Plains in the GFDL climate model using a weather forecasting approach. *Geophysical Research Letters*, *33*, L1880. https://doi.org/10.1029/2006GL027567

Koster, R. D., Dirmeyer, P. A., Guo, Z., Bonan, G., Chan, E., & Cox, P. (2004). Regions of strong coupling between soil moisture and precipitation. *Science*, *305*(5687), 1138–1140. https://doi.org/10.1126/science.1100217

Kucharik, C. J., Serbin, S. P., Vavrus, S., Hopkins, E. J., & Motew, M. M. (2010). Patterns of climate change across Wisconsin from 1950 to 2006. *Physical Geography*, *31*(1), 1–28. https://doi.org/10.2747/0272-3646.31.1.1

Lauritzen, P. H., Nair, R. D., Herrington, A. R., Callaghan, P., Goldhaber, S., Dennis, J. M., et al. (2018). NCAR release of CAM-SE in CESM2.0: A reformulation of the spectral element dynamical core in dry-mass vertical coordinates with comprehensive treatment of condensates and energy. *Journal of Advances in Modeling Earth Systems*, *10*(7), 1537–1570. https://doi.org/10.1029/2017MS001257

Lawrence, D. M., Fisher, R. A., Koven, C. D., Oleson, K. W., Swenson, S. C., Bonan, G., et al. (2019). The Community Land Model version 5: Description of new features, benchmarking, and impact of forcing uncertainty. *Journal of Advances in Modeling Earth Systems*, *11*. https://doi.org/10.1029/2018MS001583

Lawrence, D. M., Hurtt, G. C., Arneth, A., Brovkin, V., Calvin, K. V., Jones, A. D., et al. (2016). The Land Use Model Intercomparison Project (LUMIP) contribution to CMIP6: Rationale and experimental design. *Geoscientific Model Development*, *9*(9), 2973–2998. https://doi.org/10.5194/gmd-9-2973-2016

Lawrence, P. J., & Chase, T. N. (2010). Investigating the climate impacts of global land cover change in the community climate system model. *International Journal of Climatology*, *30*(13), 2066–2087. https://doi.org/10.1002/joc.2061

Lawrence, P. J., Feddema, J. J., Bonan, G. B., Meehl, G. A., O'Neill, B. C., Oleson, K. W., et al. (2012). Simulating the biogeochemical and biogeophysical impacts of transient land cover change and wood harvest in the Community Climate System Model (CCSM4) from 1850 to 2100. *Journal of Climate*, *25*(9), 3071–3095. https://doi.org/10.1175/JCLI-D-11-00256.1

Lawrence, P. J., Lawrence, D. M., & Hurtt, G. C. (2018). Attributing the carbon cycle impacts of CMIP5 historical and future land use and land cover change in the Community Earth System Model (CESM1). *Journal of Geophysical Research: Biogeosciences*, *123*, 1732–1755. https://doi.org/10.1029/2017JG004348

Lee, X., Goulden, M. L., Hollinger, D. Y., Barr, A., Black, T. A., Bohrer, G., et al. (2011). Observed increase in local cooling effect of deforestation at higher latitudes. *Nature*, *479*(7373), 384–387. https://doi.org/10.1038/nature10588

Leibensperger, E. M., Mickley, L. J., Jacob, D. J., Chen, W. T., Seinfeld, J. H., Nenes, A., et al. (2012). Climatic effects of 1950–2050 changes in US anthropogenic aerosols-Part 2: Climate response. *Atmospheric Chemistry and Physics*, *12*(7), 3349–3362. https://doi.org/10.5194/acp-12-3349-2012

Lejeune, Q., Seneviratne, S. I., Davin, E. L., Lejeune, Q., Seneviratne, S. I., & Davin, E. L. (2017). Historical land-cover change impacts on climate: Comparative assessment of LUCID and CMIP5 multimodel experiments. *Journal of Climate*, *30*(4), 1439–1459. https://doi.org/10.1175/JCLI-D-16-0213.1

Li, X., Chen, H., Wei, J., Hua, W., Sun, S., Ma, H., et al. (2018). Inconsistent responses of hot extremes to historical land use and cover change among the selected CMIP5 models. *Journal of Geophysical Research: Atmospheres*, *123*, 3497–3512. https://doi.org/10.1002/2017JD028161

Li, Y., Zhao, M., Motesharrei, S., Mu, Q., Kalnay, E., & Li, S. (2015). Local cooling and warming effects of forests based on satellite observations. *Nature Communications*, *6*(1). https://doi.org/10.1038/ncomms7603

Lin, Y., Dong, W., Zhang, M., Xie, Y., Xue, W., Huang, J., & Luo, Y. (2017). Causes of model dry and warm bias over central U.S. and impact on climate projections. *Nature Communications*, *8*(1). https://doi.org/10.1038/s41467-017-01040-2

Ma, H.-Y., Klein, S. A., Xie, S., Zhang, C., Tang, S., Tang, Q., et al. (2018). CAUSES: On the role of surface energy budget errors to the warm surface air temperature error over the central United States. *Journal of Geophysical Research: Atmospheres*, *123*, 2888–2909. https://doi.org/10.1002/2017JD027194

Mahmood, R., Pielke, R. A., Hubbard, K. G., Niyogi, D., Dirmeyer, P. A., McAlpine, C., et al. (2014). Land cover changes and their biogeophysical effects on climate. *International Journal of Climatology*, *34*(4), 929–953. https://doi.org/10.1002/joc.3736

Meehl, G. A., Arblaster, J. M., Branstator, G., Meehl, G. A., Arblaster, J. M., & Branstator, G. (2012). Mechanisms contributing to the warming hole and the consequent U.S. east-west differential of heat extremes. *Journal of Climate*, *25*(18), 6394–6408. https://doi.org/10.1175/JCLI-D-11-00655.1

Mei, R., Wang, G., Mei, R., & Wang, G. (2012). Summer land-atmosphere coupling strength in the United States: Comparison among observations, reanalysis data, and numerical models. *Journal of Hydrometeorology*, *13*(3), 1010–1022. https://doi.org/10.1175/JHM-D-11-075.1

Morcrette, C. J., Van Weverberg, K., Ma, H. Y., Ahlgrimm, M., Bazile, E., Berg, L. K., et al. (2018). Introduction to CAUSES: Description of weather and climate models and their near-surface temperature errors in 5 day hindcasts near the Southern Great Plains. *Journal of Geophysical Research: Atmospheres*, *123*, 2655–2683. https://doi.org/10.1002/2017JD027199

Mueller, N. D., Butler, E. E., McKinnon, K. A., Rhines, A., Tingley, M., Holbrook, N. M., & Huybers, P. (2016). Cooling of US Midwest summer temperature extremes from cropland intensification. *Nature Climate Change*, *6*(3), 317–322. https://doi.org/10.1038/nclimate2825

Myhre, G., Shindell, D., Bréon, F.-M., Collins, W., Fuglestvedt, J., & Huang, J. (2013). In T. F. Stocker, et al. (Eds.), *Climate change 2013: The physical science basis. Contribution of Working Group I to the Fifth Assessment Report of the Intergovernmental Panel on Climate Change*. (pp. 659–740). Cambridge, UK: Cambridge University Press.

Parton, W. J., Gutmann, M. P., & Ojima, D. (2007). Long-term trends in population, farm income, and crop production in the Great Plains. *Bioscience*, *57*(9), 737–747. https://doi.org/10.1641/B570906

Partridge, T. F., Winter, J. M., Osterberg, E. C., Hyndman, D. W., Kendall, A. D., & Magilligan, F. J. (2018). Spatially distinct seasonal patterns and forcings of the U.S. warming hole. *Geophysical Research Letters*, *45*, 2055–2063. https://doi.org/10.1002/2017GL076463

Pielke, R. A., Pitman, A., Niyogi, D., Mahmood, R., McAlpine, C., Hossain, F., et al. (2011). Land use/land cover changes and climate: modeling analysis and observational evidence. *Wiley Interdisciplinary Reviews: Climate Change*, *2*(6), 828–850. https://doi.org/10.1002/wcc.144

Pitman, A. J., de Noblet-Ducoudré, N., Cruz, F. T., Davin, E. L., Bonan, G. B., Brovkin, V., et al. (2009). Uncertainties in climate responses to past land cover change: First results from the LUCID intercomparison study. *Geophysical Research Letters*, *36*, L14814. https://doi.org/10.1029/2009GL039076

Portmann, R. W., Solomon, S., & Hegerl, G. C. (2009). Spatial and seasonal patterns in climate change, temperatures, and precipitation across the United States. *Proceedings of the National Academy of Sciences of the United States of America*, *106*(18), 7324–7329. https://doi.org/10.1073/pnas.0808533106

Prein, A. F., Langhans, W., Fosser, G., Ferrone, A., Ban, N., Goergen, K., et al. (2015). A review on regional convection-permitting climate modeling: Demonstrations, prospects, and challenges. *Reviews of Geophysics*, *53*, 323–361. https://doi.org/10.1002/2014RG000475

Prein, A. F., Liu, C., Ikeda, K., Bullock, R., Rasmussen, R. M., Holland, G. J., & Clark, M. (2017). Simulating North American mesoscale convective systems with a convection-permitting climate model. *Climate Dynamics*, 1–16. https://doi.org/10.1007/s00382-017-3993-2

Prein, A. F., Liu, C., Ikeda, K., Trier, S. B., Rasmussen, R. M., Holland, G. J., & Clark, M. P. (2017). Increased rainfall volume from future convective storms in the US. *Nature Climate Change*, *7*(12), 880–884. https://doi.org/10.1038/s41558-017-0007-7

Qian, Y., Huang, M., Yang, B., & Berg, L. K. (2013). A modeling study of irrigation effects on surface fluxes and land-air-cloud interactions in the Southern Great Plains. *Journal of Hydrometeorology*, *14*(3), 700–721. https://doi.org/10.1175/JHM-D-12-0134.1

Rhoades, A. M., Ullrich, P. A., & Zarzycki, C. M. (2018). Projecting 21st century snowpack trends in western USA mountains using variable-resolution CESM. *Climate Dynamics*, *50*(1–2), 261–288. https://doi.org/10.1007/s00382-017-3606-0

Seneviratne, S. I., Wartenburger, R., Guillod, B. P., Hirsch, A. L., Vogel, M. M., Brovkin, V., et al. (2018). Climate extremes, land-climate feedbacks and land-use forcing at 1.5°C. *Philosophical Transactions of the Royal Society A: Mathematical, Physical and Engineering Sciences*, *376*(2119). https://doi.org/10.1098/rsta.2016.0450

Shevliakova, E., Pacala, S. W., Malyshev, S., Hurtt, G. C., Milly, P. C. D., Caspersen, J. P., et al. (2009). Carbon cycling under 300 years of land use change: Importance of the secondary vegetation sink. *Global Biogeochemical Cycles*, *23*(2). https://doi.org/10.1029/2007GB003176

Song, F., Feng, Z., Leung, L. R., Houze, R. A. Jr., Wang, J., Hardin, J., & Homeyer, C. R. (2019). Contrasting spring and summer large-scale environments associated with mesoscale convective systems over the U.S. Great Plains. *Journal of Climate*, *32*(20), 6749–6767. https://doi.org/10.1175/jcli-d-18-0839.1

Unger, N. (2014). Human land-use-driven reduction of forest volatiles cools global climate. *Nature Climate Change*, *4*(10), 907–910. https://doi.org/10.1038/nclimate2347

Van Weverberg, K., Morcrette, C. J., Petch, J., Klein, S. A., Ma, H. Y., Zhang, C., et al. (2018). CAUSES: Attribution of surface radiation biases in NWP and climate models near the U.S. Southern Great Plains. *Journal of Geophysical Research: Atmospheres*, *123*, 3612–3644. https://doi.org/10.1002/2017JD027188

Varble, A., Zipser, E. J., Fridlind, A. M., Zhu, P., Ackerman, A. S., Chaboureau, J. P., et al. (2014). Evaluation of cloud-resolving and limited area model intercomparison simulations using twp-ice observations: 2. Precipitation microphysics. *Journal of Geophysical Research: Atmospheres*, *119*, 13,919–13,945. https://doi.org/10.1002/2013JD021372

Williams, I. N., Lu, Y., Kueppers, L. M., Riley, W. J., Biraud, S. C., Bagley, J. E., & Torn, M. S. (2016). Land-atmosphere coupling and climate prediction over the U.S. Southern Great Plains. *Journal of Geophysical Research: Atmospheres*, *121*, 12,125–12,144. https://doi.org/10.1002/2016JD025223

Williams, I. N., & Torn, M. S. (2015). Vegetation controls on surface heat flux partitioning, and land-atmosphere coupling. *Geophysical Research Letters*, *42*, 9416–9424. https://doi.org/10.1002/2015GL066305

Wu, C., Liu, X., Lin, Z., Rhoades, A. M., Ullrich, P. A., Zarzycki, C. M., et al. (2017). Exploring a variable-resolution approach for simulating regional climate in the Rocky Mountain region using the VR-CESM. *Journal of Geophysical Research: Atmospheres*, *122*, 10,939–10,965. https://doi.org/10.1002/2017JD027008

Yang, Q., Houze, R. A., Leung, L. R., & Feng, Z. (2017). Environments of long-lived mesoscale convective systems over the central United States in convection permitting climate simulations. *Journal of Geophysical Research: Atmospheres*, *122*(24), 13,288–13,307. https://doi.org/10.1002/2017JD027033

Yang, Z., Dominguez, F., Gupta, H., Zeng, X., & Norman, L. (2016). Urban effects on regional climate: A case study in the Phoenix and Tucson "sun corridor". *Earth Interactions*, *20*(20), 1–25. https://doi.org/10.1175/EI-D-15-0027.1

Yang, Z., Qian, Y., Liu, Y., Berg, L. K., Hu, H., Dominguez, F., et al. (2019). Irrigation impact on water and energy cycle during dry years over the United States using convection-permitting WRF and a dynamical recycling model. *Journal of Geophysical Research: Atmospheres*, *124*(21), 11,220–11,241. https://doi.org/10.1029/2019JD030524

Zarzycki, C. M., & Jablonowski, C. (2014). A multidecadal simulation of Atlantic tropical cyclones using a variable-resolution global atmospheric general circulation model. *Journal of Advances in Modeling Earth Systems*, *6*(3), 805–828. https://doi.org/10.1002/2014MS000352

Zarzycki, C. M., Levy, M. N., Jablonowski, C., Overfelt, J. R., Taylor, M. A., & Ullrich, P. A. (2014). Aquaplanet experiments using CAM's variable-resolution dynamical core. *Journal of Climate*, *27*(14), 5481–5503. https://doi.org/10.1175/JCLI-D-14-00004.1

Zhang, C., Xie, S., Klein, S. A., Ma, H. Y., Tang, S., Van Weverberg, K., et al. (2018). CAUSES: Diagnosis of the summertime warm bias in CMIP5 climate models at the ARM Southern Great Plains site. *Journal of Geophysical Research, Atmospheres*, *123*, 2968–2992. https://doi.org/10.1002/2017JD027200

Zhang, G. J., & McFarlane, N. A. (1995). Sensitivity of climate simulations to the parameterization of cumulus convection in the Canadian Climate Centre general circulation model. *Atmosphere-Ocean*, *33*(3), 407–446. https://doi.org/10.1080/07055900.1995.9649539